SCIENCE AND TECHNOLOGY OF ADVANCED MATERIALS
2023, VOL. 24, NO. 1, 2210723
https://doi.org/10.1080/14686996.2023.2210723

Taylor & Francis
Taylor & Francis Group

FOCUS ISSUE REVIEW

OPEN ACCESS Check for updates

Structural water molecules dominated p band intermediate states as a unified model for the origin on the photoluminescence emission of noble metal nanoclusters: from monolayer protected clusters to cage confined nanoclusters

Bo Peng[a], Jia-Feng Zhou[a], Meng Ding[a], Bing-Qian Shan[a], Tong Chen[a] and Kun Zhang[a,b,c,d]

[a]Shanghai Key Laboratory of Green Chemistry and Chemical Processes, College of Chemistry and Molecular Engineering, East China Normal University, Shanghai, China;
[b]Laboratoire de chimie, Ecole Normale Supérieure de Lyon, Institut de Chimie de Lyon, Université de Lyon, Lyon, France;
[c]Shandong Provincial Key Laboratory of Chemical Energy Storage and Novel Cell Technology, School of Chemistry and Chemical Engineering, Liaocheng University, Liaocheng, Shandong, PR China;
[d]Institute of Eco-Chongming, Shanghai, China

ABSTRACT

In the past several decades, noble metal nanoclusters (NMNCs) have been developed as an emerging class of luminescent materials due to their superior photo-stability and biocompatibility, but their luminous quantum yield is relatively low and the physical origin of the bright photoluminescence (PL) of NMNCs remain elusive, which limited their practical application. As the well-defined structure and composition of NMNCs have been determined, in this mini-review, the effect of each component (metal core, ligand shell and interfacial water) on their PL properties and corresponded working mechanism were comprehensively introduced, and a model that structural water molecules dominated *p* band intermediate state was proposed to give a unified understanding on the PL mechanism of NMNCs and a further perspective to the future developments of NMNCs by revisiting the development of our studies on the PL mechanism of NMNCs in the past decade.

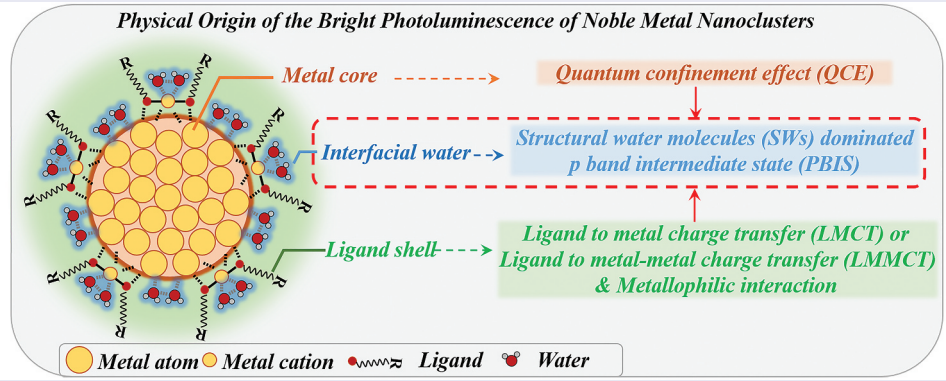

ARTICLE HISTORY
Received 27 January 2023
Revised 29 April 2023
Accepted 29 April 2023

KEYWORDS
Noble metal nanoclusters; photoluminescence mechanism; interfacial water; structural water molecules; *p* band intermediate state; aggregation-induced emission; nanocatalysis; chirality

1. Introduction

'Atoms on a small scale behave like nothing on a large scale, for they satisfy the laws of quantum mechanics'. As early as 1959, physicist *Richard Phillip Feynman* proposed the idea of arranging atoms on a microscopic scale and predicted the unique properties of small-size materials compared to macroscopic ones [1] With the continuous improvement of synthesis methodology and characterization methods, the synthesis of nanomaterials has achieved rapid development in the past two decades. A prominent case is that nano-sized noble metal (nanoparticles or nanoclusters) with magic atom numbers, also called the atomically precise NCs, can be synthesized at the molecular level [2–7], and as expected, these tiny particles or clusters exhibited unique electronic and optical properties, such as molecule-like energy gaps [8–13], photoluminescence (PL) [6,14–27], catalytic properties [28–39] and chirality [40–47]. In particular, the PL phenomenon is one of the most intriguing characteristics of NMNCs compared to bulk metals, which fascinated scientists in many areas of research

CONTACT Kun Zhang kzhang@chem.ecnu.edu.cn Shanghai Key Laboratory of Green Chemistry and Chemical Processes, College of Chemistry and Molecular Engineering, East China Normal University, Shanghai 200062, China

and applications [48,49], but the luminous quantum yield of NMNCs is still relatively low [21]. These prominent optical properties of NMNCs were initially attributed to the quantum size confinement effect [14,50], whereas, the efficiency and wavelength of the luminescence of NMNCs was not only dictated by the size, composition and valence state of metal core [51–53], but also by the type, architecture of surface ligands [17,54–61], *etc*. Although the atomic structure of NMNCs can be determined [2,62], the elucidation on the origin of the optoelectronic properties of metal NCs is still diverse and even contradictory [21,63]. Thus it is highly important to describe the chemical and physical origin, which can guide a rational synthesis of highly luminescent NMNCs. This review will therefore mainly focus on the summary of the PL mechanism of NMNCs and give a further perspective to the future developments of NMNCs based on the literature survey and our long-term studies in the past decade, and the content of this review is organized as follows: in the first section, we briefly introduce the composition and structure of NMNCs and classify the NMNCs into two categories: organic ligand protected NMNCs and inorganic scaffold confined NMNCs. The second section describes the effect of each component (metal core, ligand shell and interfacial water) of NMNCs on the PL properties and corresponded working mechanism (quantum confinement effect (QCE), ligand to metal charge transfer (LMCT) or ligand to metal-metal charge transfer (LMMCT) and metallophilic interaction beyond aggregation-induced emission (AIE) effect, *etc*.). In the last section, the historical development of our studies on the PL mechanism of NMNCs is introduced, and a model that structural water molecules (SWs) dominated PL of NMNCs is addressed. We hope that this reviews will provide new insights to understanding not only the PL mechanism but also other unique properties (such as catalysis, chirality, *etc*.) of NMNCs and other low-dimensional nanomaterials (carbon dots, AIEgens, semiconductor quantum dots, *etc*.).

2. The composition and structure of NMNCs

The bulk metal has a continuous energy level structure and exhibits good electrical conductivity and metallic luster. When the size of metals is reduced to the nanometer level (2–100 nm), the density of states (DOS) in the band decreases [64], metal nanoparticles (NPs) exhibit obvious surface plasma resonance (SPR) absorption, which is caused by the collective oscillation of the conduction band electrons under optical radiation [65], at which time the noble metal NPs still have a quasi-continuous energy level structure that the gap between the highest occupied and the lowest unoccupied state (called the Kubo gap δ) is still less than thermal energy (kT), showing the properties of a metallic state [64]. When the size of noble metal NPs further decrease to less than 2 nm, the DOS in the band further decreases and the Kubo gap is larger than thermal energy (kT). Noble metal NPs at this scale are generally called noble metal nanoclusters (nanoclusters, NCs), which bridge the gap between organometallics and nanocrystals and thus show discrete energy level structure and molecule-like absorption [3–5,16,21,66–70]. Figure 1(a) is a schematic diagram of evolution of the energy level structure of metals as a function of size. And specifically, the critical number of gold atoms for a metallic state NCs has been determined recently, in which atomically precise gold nanoclusters $Au_{246}(SR)_{80}$ is nonmetallic but $Au_{279}(SR)_{84}$ (M_nL_m, n and m represent the number of metal atoms and ligands, respectively. SR: thiolate) is metallic (Figure 1(b)) [71,72].

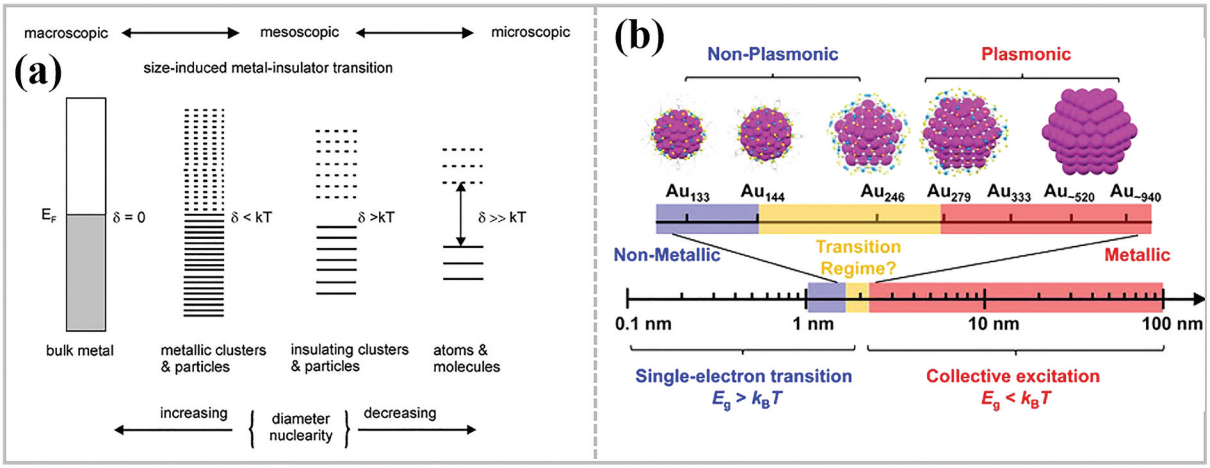

Figure 1. (a) Schematic illustration of the energy level of metal with decreased size [64]. Reproduced with permission from ref. [64]. Copyright 2006 the royal society of chemistry. (b) Schematic diagram of the grand transition from nonmetallic state to metallic state in Au NCs [71]. Reproduced with permission from ref. [7]. Copyright 2021, American chemical society.

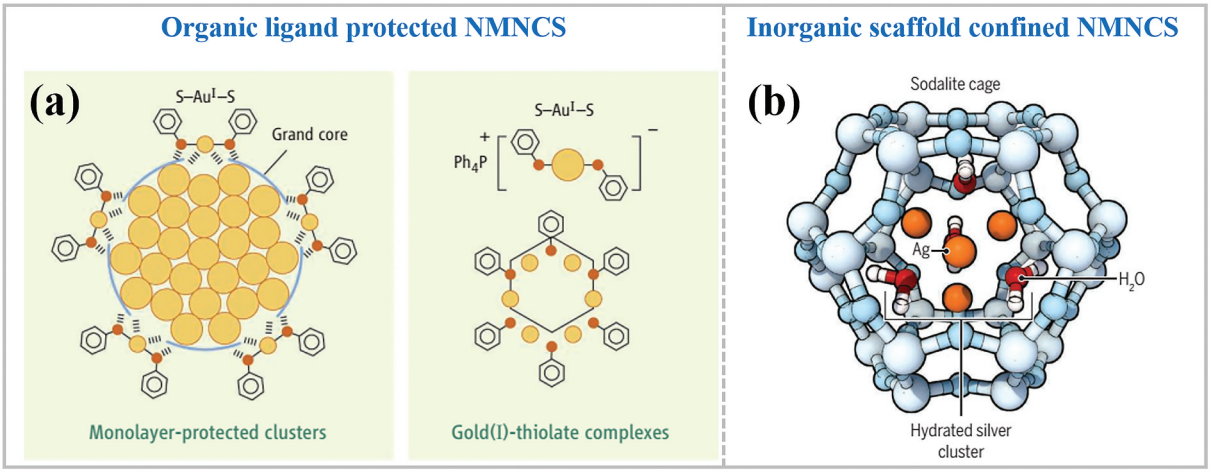

Figure 2. Schematic representation of (a) monolayer-protected Au NCs, Au(I)-thiolate complexes (Au(i)-SRs) [73] and (b) a hydrated Ag_4 cluster inside a sodalite zeolite cage [74]. Reproduced with permission from ref. [73]. Copyright 2007 American association for the advancement of science and ref. [74]. Copyright 2018 American association for the advancement of science.

Bare NMNCs are not stable in solution due to their high surface energy, thus NMNCs are generally protected by organic or inorganic scaffold. According to the difference in the properties of the protective scaffold on the surface of noble metal NCs, herein, noble metal NCs can be mainly divided into two categories: one is organic ligand protected NMNCs [2,73]; the other is inorganic scaffold confined NMNCs [6,74]. Both type of NMNCs have well-defined structure and compositions, as shown in Figure 2, organic ligand protected NMNCs mainly comprised by zero-valent metal core and metal(I)-ligand complex shell on the surface (Figure 2(a)): The crystal structure and the number of gold atoms and ligands can be accurately analyzed at the atomic level, and the NMNCs protected by atomically accurate organic ligands can be synthesized with molecular-level purity [3,4]. The inorganic scaffold confined NMNCs mainly consist of metal cores, adsorbed water molecules, and confined pores of inorganic templates (Figure 2(b)): No matter organic ligand protected NMNCs or inorganic scaffold confined NMNCs, each component of NMNCs shows a significant impact on the optical properties of NMNCs, which complicated the investigation on the PL mechanism of NMNCs. Besides, there are many different photophysical process occurring in NMNCs, mainly including radiative relaxation pathways (*e.g.* near-infrared fluorescence (NIRF)) and non-radiative pathways (*e.g.* heat, photoacoustic (PA) and reactive oxygen species (ROS)) as shown in Figure 3(a) (take ligand protected gold nanoclusters as an example), only radiative relaxation pathways (occurring from surface, core and triplet states) can lead to a rich and color-tunable PL of NMNCs [49]. For instance, the visible and near-infrared emissions in typical $[Au_{25}(SR)_{18}]^-$ nanoclusters have been recently attributed to the core-shell charge transfer state and the electron decay of the Au_{13} core excited state, respectively (Figure 3(b)) [75]. The authors conclude that these low-energy decay dynamics of Au NCs follows the multi-photon process, which could be found the interesting applications in the field of oncology [49]. Although a lot of types of NMNCs differed in the metal and/or ligand have been reported in the literature, the luminescence mechanism of them could follow the same principle, in this review, we will mainly focus on the systems of gold and silver-based nanoclusters, in some cases, the metal(I)-thiolates complexes are also introduced. In the following section 2 and section 3, we will separately introduce the effect of each component (metal core, ligand shell and interfacial water) of NMNCs on the PL properties but will not strictly separate these nanosystems to explain the origin of the PL and try to give a unified understanding of the luminescence mechanism of NMNCs.

2. Luminescence mechanism of NMNCs

2.1 The effect of metal core

In 1969, Mooradian firstly observed the photoluminescence of gold and copper films with the emission energy centered at 2.2 and 2.0 eV respectively (Figure 4(a)) [76], but the quantum yields were extremely low (~10^{-10}), as bulk metal has a continuous energy level structure within the band, the emission was therefore attributed to the interband transition between electrons in conduction-band states below the Fermi level and holes in the d bands (Figure 4(b)). The PL intensity of bulk gold films can be increased by about 8 times through improving the roughness of the metal surface [78], but when the size of gold was further reduced to gold nanorods with a diameter of 20 nm, its fluorescence quantum yield was increased about one million times [79]. The size of metal obviously showed a more prominent effect on

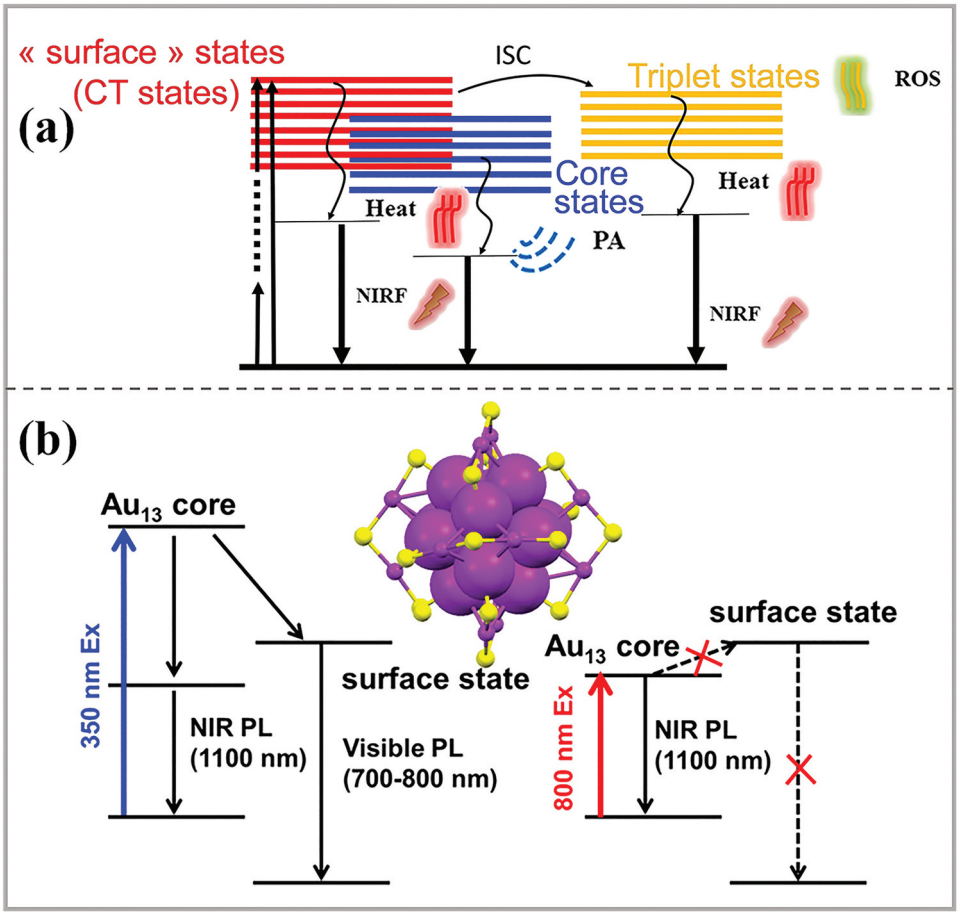

Figure 3. (a) Proposed mechanism for relaxation pathways in protected gold nanoclusters following (multi) photon absorption. NIRF: NIR fluorescence, PA: Photoacoustic, ROS: Reactive oxygen species, ISC: Inter system crossing [49]. (b) Mechanism of emissions in $[Au_{25}(SR)_{18}]^-$ nanoclusters [75]. Reproduced with permission from ref. [75]. Copyright 2021 American chemical society.

its PL properties, whereas, the luminescence properties of bulk metal and large metal NPs did not attract much more attention from photochemists and photophysicists due to their low quantum yields ($<10^{-4}$) at this stage. With the development of synthesis methodology and characterization methods, smaller or even atomically precise metal NCs can be facilely synthesized, and these metal NCs exhibited more unique optical properties [3–5,16,21,66–70]. In 1998, Wilcoxon et al. investigated the size effect on the luminescence properties of nanosize gold clusters through liquid chromatographic analysis [24], they demonstrated that the large gold clusters with the size of 15 nm are non-luminescent, while the smaller gold clusters with the size of 5 nm or 2.5 nm can exhibit relatively intense visible photoluminescence with quantum yield of $10^{-4} \sim 10^{-5}$, notably, the emission is also dependent on the nature of the metal NCs surface (capping ligand), and the large, nonemitting gold nanoparticles can also be made luminescent by partial dissolution using potassium cyanide. In 2001, Huang and Murray prepared water-soluble Au NCs with different sizes (1.8 nm, 2.2 nm, 3.1 nm and 3.9 nm) by etching [26], only Au NCs with the size of 1.8 nm showed intense fluorescence, and its quantum yield reached 0.3%, while Au NCs with other sizes were not fluorescent; similarly, the efficiency and wavelength of the luminescence was also dependent on the surface ligand. At this stage, the luminescence mechanism of Au NCs is still considered to be consistent with the luminescence mechanism of bulk metals, that is the band gap transitions between the fully filled $5d^{10}$ band of a metal such as gold and the underfilled $6sp^1$ band (Figure 4(b)), but the surface ligand was highlighted to influence the efficiencies and energies of the *6sp* emitter states, the size effect on the luminescence properties of nano-size gold NCs is still not well-elucidated. Whetten et al. isolated a series of Au NCs in solution by fractional crystallization or column chromatography [50], these Au NCs are distinguished by a crystalline (or quasicrystalline) core of densely packed Au atoms, ranging in size from~1.1 nm (~40 atoms) to ~1.9 nm (~200 atoms), surrounded by surface ligand based on the characterization of mass spectrometry and high-resolution transmission electron microscopy (TEM), unlike bulk gold and large-sized Au NPs or Au NCs, Au NCs of corresponding size exhibit a size-dependent

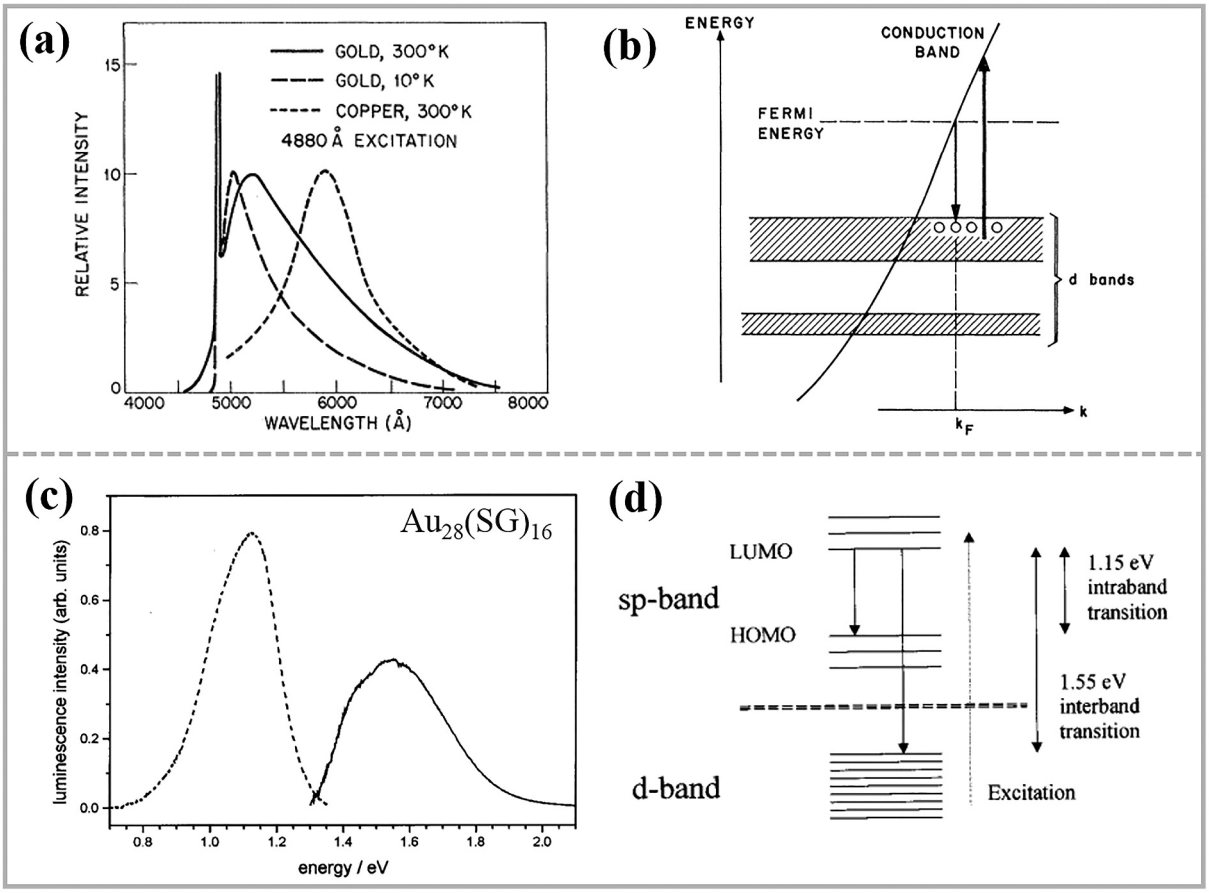

Figure 4. Photoemission spectra of (a) bulk gold and copper films and (c) gold nanoclusters $Au_{28}(SG)_{16}$ [76,77]. Schematic illustration of (b) interband and (d) intraband excitation and emission [76,77]. Reproduced with permission from ref. [76]. Copyright 1969 American physical society and ref. [77]. Copyright 2002, American chemical society.

energy level structure in the UV-Vis absorption spectrum, indicative of transitions to the discrete lowest unoccupied levels of the conduction band due to the quantum confinement effect, that is, the transitions between discrete energy levels within the *6sp* energy band (Figure 4(d)). Afterwards, Whetten et al. further investigated the luminescence properties of these molecular-like Au NCs [8,25,77,80]. The Au NCs composed of a 28-atom core and a glutathione (GSH) adsorbate layer consisting of 16 molecules exhibited two emission bands at 1.5 and 1.15 eV (Figure 4(c)), which were assigned to the recombination of the excited electron from higher excited states in the *sp* band with the hole in the lower-lying d-band (interband transition) and the relaxed radiative recombination across the gap between the highest occupied and lowest unoccupied molecular orbitals at 1.3 eV within the *sp*-conduction band (intraband transition), respectively. Thus the quantum confinement effect (QCE) was applied to account for the size effect on the luminescence properties of NMNCs. According to the mechanism of QCE, the emission wavelength of Au NCs can be tuned by changing the size of noble metal NCs. In 2002, Dickson et al. synthesized Au NCs with different sizes ($Au_5 \rightarrow Au_{31}$) using polyamide as a template [14], as-obtained Au NCs exhibit size-dependent fluorescence emission from ultraviolet to near-infrared light (Figure 5(a)), where the relationship between the emission wavelength (λ_{em}) of Au NCs and the number of gold atoms (N) approximately conforms to the relationship $\lambda_{em} = E_{Fermi}/N_{1/3}$, where E_{Fermi} represents the Fermi level of Au (Figure 5(b)). Besides, similar size-dependent optical properties was also observed in other NMNCs. For instance, Tsukuda et al. prepared glutathione (GSH) protected gold NCs by reductive decomposition of Au(I)-SG polymers [10,81], as-obtained Au NCs solution was separated into a number of fractions by polyacrylamide gel electrophoresis (PAGE), the fractionated nanoclusters are assigned to $Au_{10}(SG)_{10}$, $Au_{15}(SG)_{13}$, $Au_{18}(SG)_{14}$, $Au_{22}(SG)_{16}$, $Au_{22}(SG)_{17}$, $Au_{25}(SG)_{18}$, $Au_{29}(SG)_{20}$, $Au_{33}(SG)_{22}$, and $Au_{39}(SG)_{24}$ by electrospray ionization (ESI) mass spectrometry. As shown in Figure 5(c), these gold NCs aqueous solution shows size-dependent absorption in the UV-visible region and thus exhibited different colors in the optical images. These results are in good agreement with the quantum confinement mechanism. However, actually, most of NMNCs exhibited weak or undetectable luminescence [21], the QCE mechanism is difficult to reasonably explain the difference in the fluorescence quantum

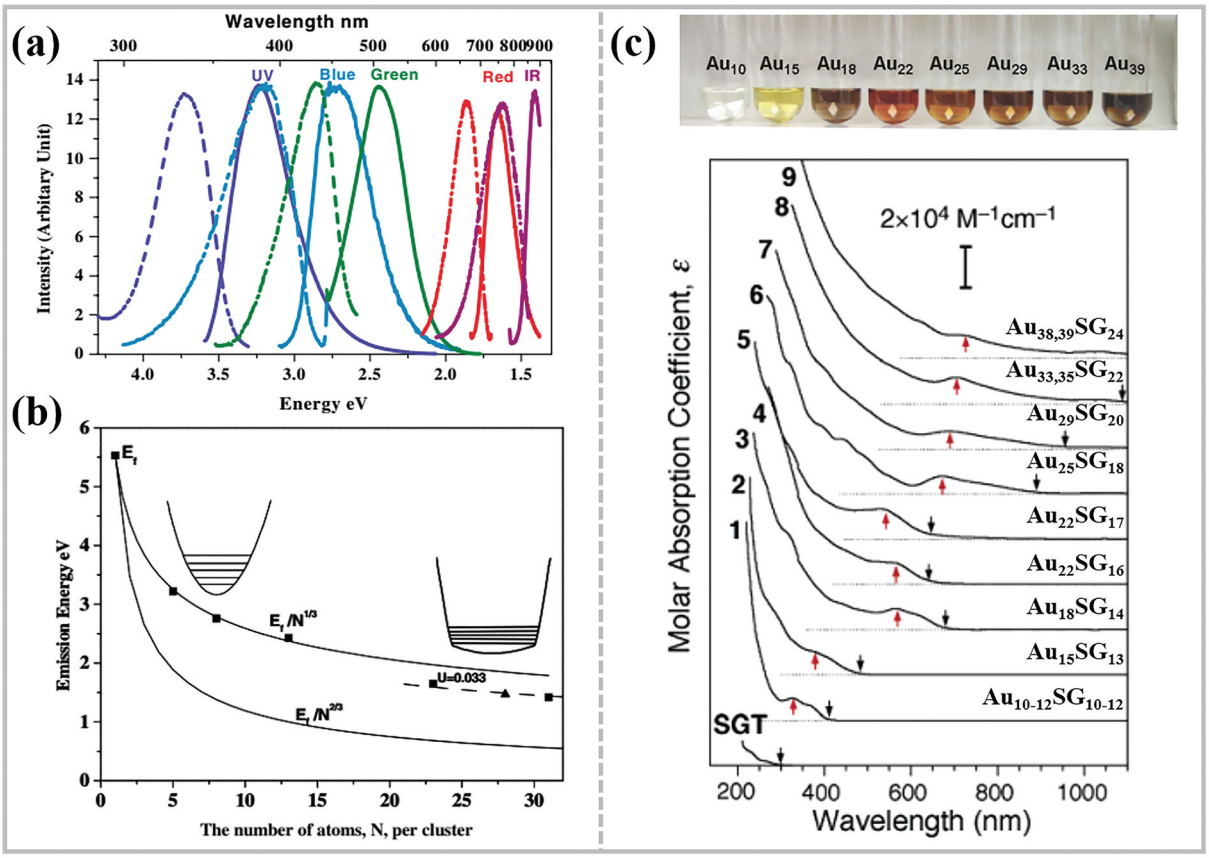

Figure 5. (a) Photoemission spectrum of Au NCs with different gold atoms. (b) Relationship between the number of gold atoms and emission energy [14]. Reproduced with permission from ref. [14]. Copyright 2004 American physical society. (c) Digital photographs (top) and optical absorption spectra (down) of aqueous solutions of Au NCs with different gold atoms [10,81]. Reproduced with permission from ref. [10]. Copyright 2005 American chemical society and ref. [81]. Copyright 2007 Wiley-VCH.

efficiency of noble metal NCs. In addition, the fluorescence emission wavelength of noble metal NCs is not always size-dependent. For example, in 2012, Xie et al. synthesized a series of atomically precise glutathione (GSH) ligand-protected noble metal NCs ($Au_{29}SG_{27}$, $Au_{30}SG_{28}$, $Au_{36}SG_{32}$, $Au_{39}SG_{35}$ and $Au_{43}SG_{37}$) [55], as the number of gold atoms increases, the fluorescence emission wavelength of Au NCs blue-shifts from 620 nm to 605 nm, the size effect of Au NCs is not obvious, and the variation of emission wavelength with size does not satisfy the QCE mechanism. Zheng et al synthesized Au NCs with the same size (~2.5 nm), but exhibited fluorescence emission at 600 nm and 810 nm, respectively, due to the different bonding modes of ligands on the surface [53]. These abnormal or conflicting experimental results indicated that the QCE mechanisms have significant limitations in explaining the luminescence properties of NMMCs, the surface ligand also shows a significant impact on the optical properties of NMNCs [63].

2.2 The effect of ligand shell

Organic ligands [3,4,21,29,68], such as small organic molecules [82], polymers [51], proteins and DNA [83–87], are typically used to control the particle size of metal core and protect tiny metal clusters from irreversible aggregation in the synthesis of NMNCs, whereas, more and more experimental results demonstrate that the optical properties of NMNCs are highly dependent on the nature and aggregation or assembly state of surface ligand. In 2004, Murray et al. investigated the ligand effect on the luminescence properties of Au NCs through the methodology of ligand exchange [9]. The PL of Au_{38} NCs was more intense after partially substituting the phenethylthiol (PhC_2SH) ligand of $Au_{38}(PhC_2S)_{24}$ by a thiol-substituted polyethylene glycol ligand ($PEG_{135}SH$) without changing the number of gold atoms, indicating that the luminescence properties of noble metal NCs are closely related to the nature of surface ligands. In 2010, Jin et al. studied in detail the role of ligand in the fluorescence of atomically monodisperse, 25-atom gold nanoclusters ($Au_{25}SR_{18}$, -SR = SC_2H_4Ph, SC_6H_{13}, $SC_{12}H_{25}$ and -SG (glutathione)) [54]. The fluorescence intensity of $Au_{25}SR_{18}$ NCs increased with the enhancement of the electron-donating ability of the ligand and the increase in the oxidation state of Au NCs (Figure 6(a,b)). The authors suggest that the surface ligands can influence the fluorescence in two different ways: (i) charge transfer from the ligands to

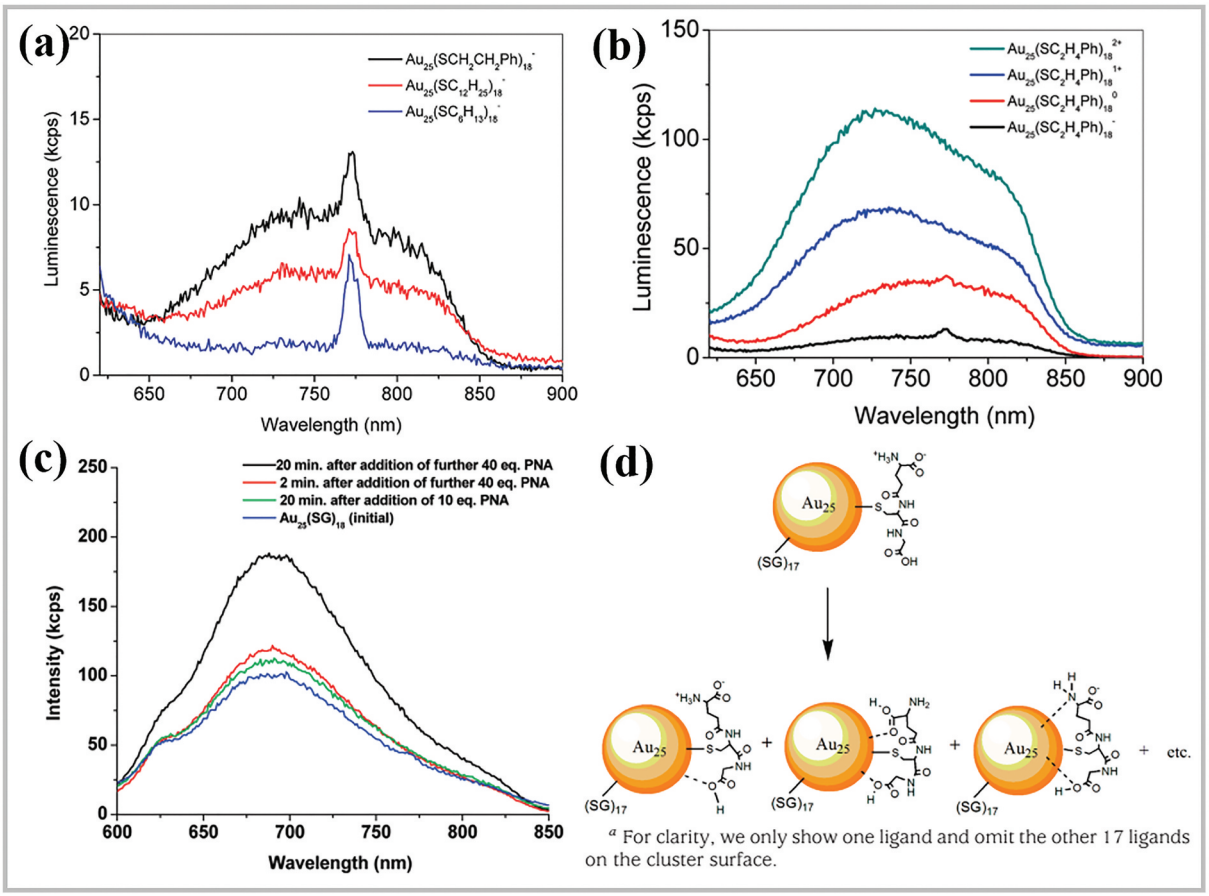

Figure 6. Photoemission spectra of Au_{25} species with different ligand (a) or different charge states (b) or the addition of PNA (c); (d) Schematic illustration of possible interactions of amine and carboxyl groups of glutathione (−SG) ligands to the gold surface [54]. Reproduced with permission from ref. [54]. Copyright 2010 American chemical society.

the metal nanoparticle core (*i.e.*, LMNCT) through the Au-S bonds, and (ii) direct donation of delocalized electrons of electron-rich atoms or groups of the ligands to the metal core (Figure 6(d)). Thus the fluorescence of Au NCs further enhanced by employing ligands (long-chain peptide nucleic acid, PNA) with electron-rich atoms and groups (Figure 6(c)), but the fluorescence efficiency of these noble metal NCs is still very low (QY < 10^{-3}). Intriguingly, in 2012, Xie et al. discovered that non-luminescent Au(I)-thiolate (Au(I)-SRs) complexes can generate strong luminescence emission after dense aggregation by either a solvent-induced or cation-induced method (Figure 7(a-d)) [55], which is reminiscent of the fluorescence enhancement phenomenon of organic chromophores in the aggregated state, namely AIE, discovered by Tang et al. in 2001 (Figure 7(e-g)) [88]. The intensity and color of the luminescence were largely determined by the degree of aggregation, the emission from the Au(I)-SRs aggregates was directly attributed to the ligand-to-metal charge transfer (LMCT) or ligand-to-metal-metal charge transfer (LMMCT) from the sulfur atom in the thiolate ligands to the Au atoms, and subsequent radiative relaxation. The authors suggested that the stronger intra- and inter-complex aurophilic Au(I)···Au(I) interactions and more restrained molecular vibrations within these Au(I)-SRs aggregates were the possible two reasons for the luminescence enhancement of Au(I)-SRs complexes in the aggregated state. Besides, based on the mechanics of AIE, the authors prepared highly luminescent Au-thiolate NCs with a Au(0)@Au(I)-thiolate core-shell structure, in which the emission wavelength of the luminescence was identical to that of Au(I)-SRs complexes, and its quantum yield can reach about~15%. These results further emphasized the crucial role of ligand or metal(I) complexes in the PL of NMNCs and inspired the researchers to reconsider the contribution of metal core and ligand in the PL of NMNCs. Note that, the d^{10} coinage metal organic chalcogenolates (MOCs) with the formula $[M(ER)]_n$, where M = Cu(I), Ag(I), Au(I) and ER = -SR, -SeR, -TeR, is also an intriguing type of luminescent materials [89–92], they can exist as oligomeric species or coordination polymers in the solution or solid state, and the photoemission of MOCs was also highly dependent on their structure and the ligand, but the PL mechanism of MOCs also remains elusive. In the follow-up research work, Xie et al. further revealed the impact of surface Au(I)-thiolate motifs on the AIE properties of Au NCs by employing a series of atomically precise glutathione coordinated Au

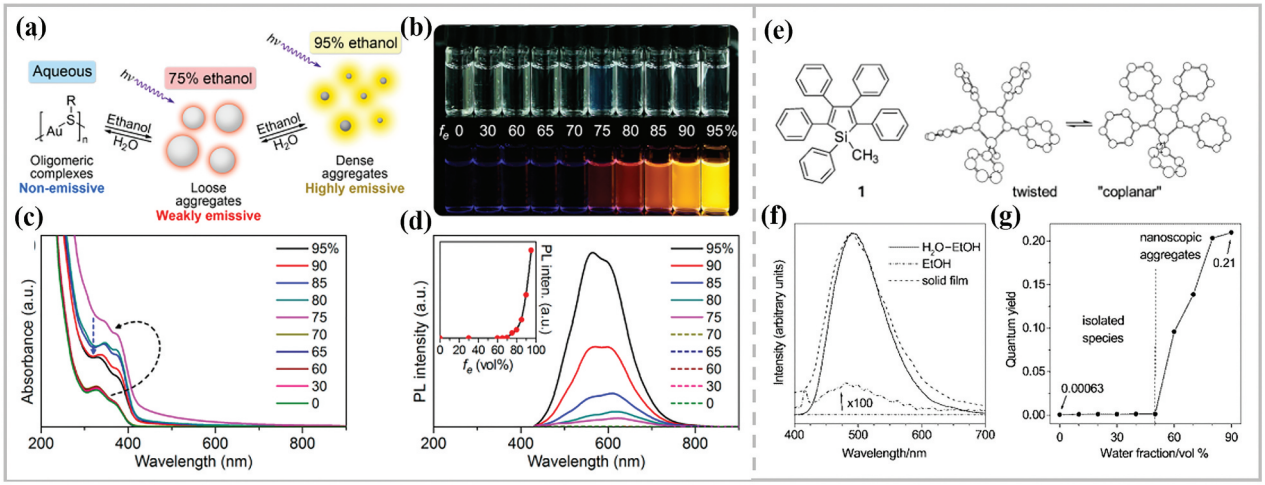

Figure 7. (a) Schematic illustration of solvent-induced AIE properties of oligomeric Au(I)-thiolate complexes. (b) Digital photos of Au(I)-thiolate complexes in mixed solvents of ethanol and water with different f_e under visible (top row) and UV (bottom row) light. (c) UV-vis absorption and (d) photoemission spectra of Au(I)-thiolate complexes in mixed solvents with different f_e. Inset: Relationship between the luminescence intensity and f_e [55]. Reproduced with permission from ref. [55]. Copyright 2012 American chemical society. (e) Molecular structure and conformational rotamers of 1; (f) PL spectra of 1 in water-ethanol mixture (90 + 10 by volume), absolute ethanol, and solid film; (g) Quantum yield of 1 vs. solvent composition of the water-ethanol mixture [88]. Reproduced with permission from ref. [88]. Copyright 2001 the royal society of chemistry.

complexes and NCs as a model ($Au_{10}SR_{10}$, $Au_{15}SR_{13}$, $Au_{18}SR_{14}$, and $Au_{25}SR_{18}$) [56]. Spectroscopic investigations show that the emission energy and emission pathway of Au NCs was highly dependent on the length or size of the Au(I)-SRs motifs (Figure 8(a,b)), Au NCs with longer Au(I)-SRs motif showed a strong AIE effect and thus exhibited an AIE-type phosphorescence with longer lifetime and higher emission energy, whereas, Au NCs with shorter Au(I)-SRs motif only exhibited an Au(0)-core-dictated fluorescence with shorter lifetime and lower emission energy (Figure 8(c)). Indeed, AIE is an effective strategy to synthesize highly luminescent NMNCs [93–99], and there is no doubt that the restriction of intramolecular motion could result in the luminescence enhancement from AIE luminogens (AIEgens) in the aggregated state due to the decrease in the probability of non-radiative relaxation of the excited states [100,101]. Whereas, the origin of the emission of metal(I)-complexes [94] and other organic small molecules without conjugated chromophore [102] but showing AIE effect is still mysterious [103], the metallophilic

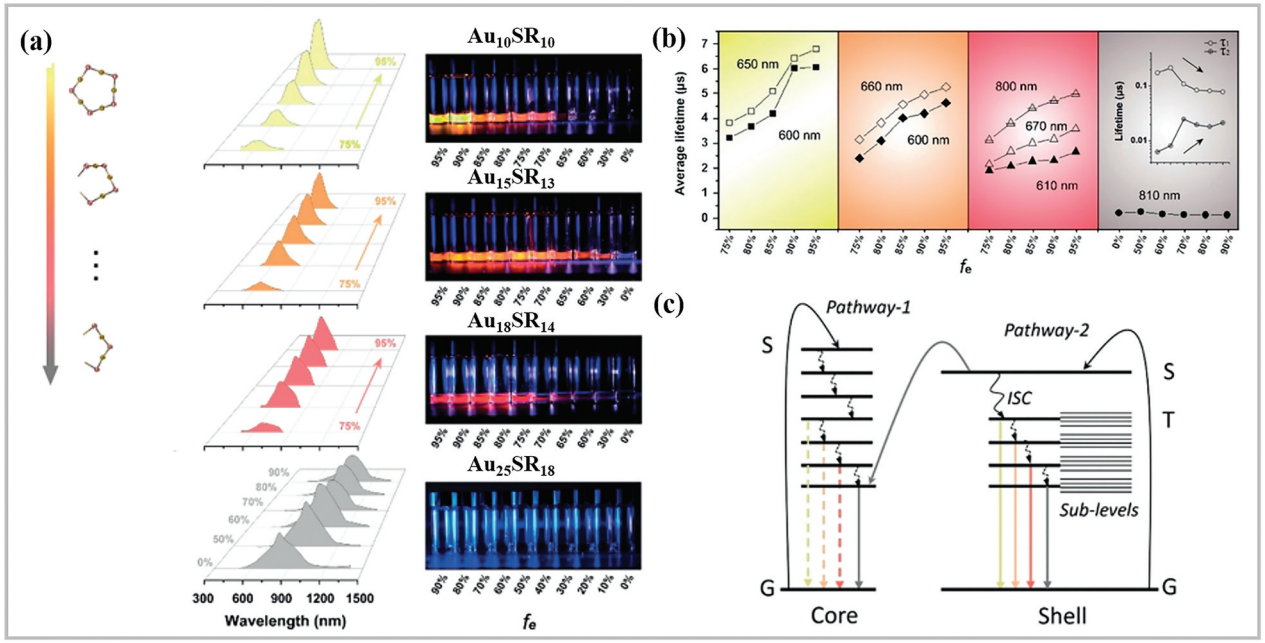

Figure 8. (a) Aggregation-induced emission of Au NCs with decreased length of Au(I)-SRs motifs (from top to bottom). (b) Summary of the corresponding emission lifetimes. (c) Schematic illustration of the excited-state relaxation dynamics of Au NCs [56]. Reproduced with permission from ref. [56]. Copyright 2020 Wiley-VCH.

interaction, a specific intra- and intermolecular bonding between closed-shell metal centers such as $Au^+[5d_{10}]$ [104], were generally involved in the accounting for the AIE effect of metal(I)-complexes, however, the physical origin of the metallophilic interaction and the relationship between metallophilic interaction and optical properties of metal(I)-complexes aggregates are still unclear.

2.3 The effect of interfacial water

In addition to traditional organic ligand, NMNCs can also be protected by the inorganic scaffolds [105,106], such as glass [107,108], metal-organic frameworks (MOFs) [105] and zeolites [109]. These inorganic materials with uniform microporous structure can provide strong physical confinement effect on NMNCs after encapsulating NMNCs inside their void nanospaces. Typically, crystalline zeolite with molecularly sized cages are perfectly suited to accommodate NMNCs, but in fact only a very small part of zeolite encapsulated NMNCs can observe bright photoluminescence [19,20,109–111], and unexpectedly, their optical properties were highly dependent on the hydration status of NMNCs [112]. In 2009, Vosch et al. prepared highly luminescent silver nanoclusters (Ag NCs) through thermal treatment of Ag^+-exchanged LTA- and FAU-type aluminosilicate zeolites (Figure 9(a)) [19], the luminescence properties of these Ag NCs within zeolite matrixes were dependent on the zeolite topology, the silver loading and the nature of counterions [19,113,114]. The dominant emission bands of Ag NCs in LTA-type zeolite were situated around 550 nm and 690 nm for the samples with, respectively, low and high silver content, whereas, Ag NCs in FAU-type zeolites only exhibited a broad emission band centered at around 550 nm. These emitters with characteristic luminescence colors were primarily ascribed to Ag_x^+ clusters with different number of silver atoms within zeolites, typically Ag_3^+ cluster for emitters at 550 nm and Ag_6^+ cluster for emitters at 690 nm, based on the analysis of the fluorescence and electron spin resonance properties. Besides, the cations balanced the negative charge of aluminosilicate can also efficiently tune the emission color of these Ag NCs. For instance, Steele et al. observed that the gradual incorporation of Li^+ into LTA zeolites (counterions: Na^+) resulted a successive hypsochromic shift of the emission energy from 2.05 eV (605 nm) to 2.43 eV (510 nm) of these confined Ag NCs [113], but the excitation maxima and external quantum efficiency remain nearly constant

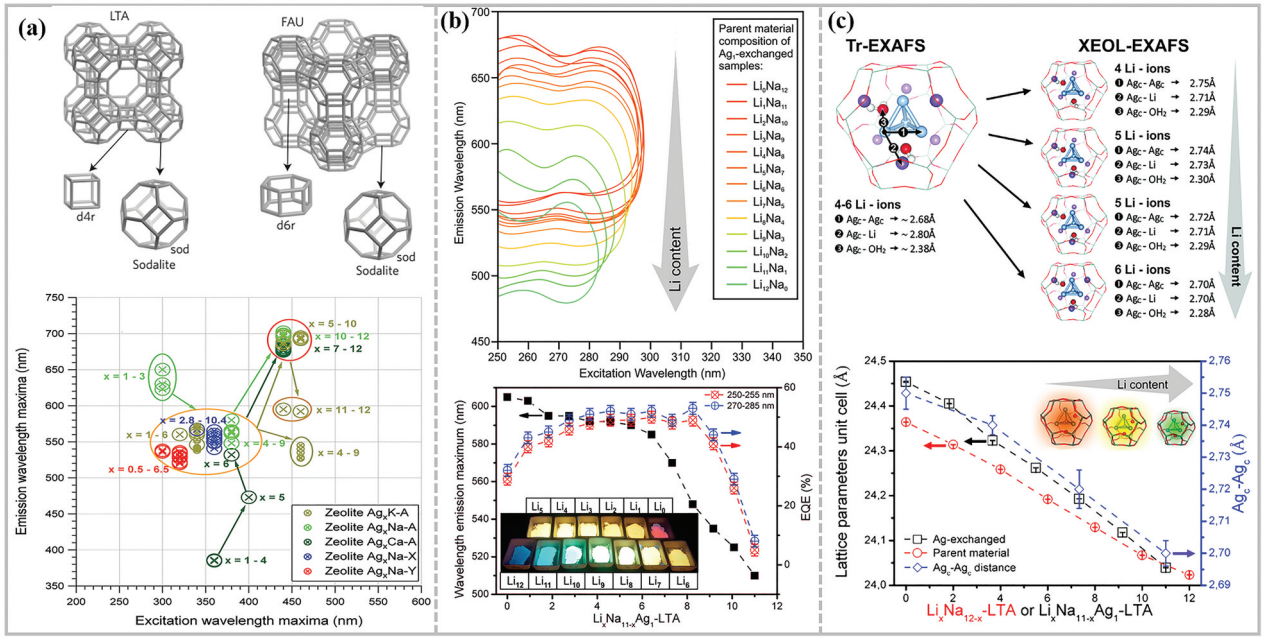

Figure 9. (a) Schematic of the LTA and FAU zeolite frameworks and their building blocks (top) [20], position of the most pronounced luminescence bands of the heat treated silver-exchanged zeolites (down) [19]. Reproduced with permission from ref. [19]. Copyright 2009 American Chemical Society and ref. [20]. Copyright 2016 springer nature. (b) 2D emission and excitation profiles of the different hydrated Ag_1-exchanged LTA zeolite samples, with a parent Li_xNa_{12-x}-LTA composition as depicted in the legend (top), maximal emission wavelength and EQEs of the $Ag_1Li_xNa_{11-x}$-LTA zeolites depending on the Li content of the exact composition of the luminescent zeolite (down). Inset shows the emission color of the different samples [113]. (c) Schematic representation of the changes observed for the ground and excited states of the tetrahedral Ag clusters confined inside the sodalite cages of the LTA zeolite as determined by Tr- (left) and XEOL-EXAFS (right), respectively (top), changes to lattice parameters of unit cell of Ag_1- and nonexchanged Li_xNa_{12-x}-LTA zeolites and Ag_c-Ag_c distances of the tetrahedral Ag clusters compared to Li-Na content of the Ag_1-exchanged Li_xNa_{12-x}-LTA zeolites (down) [113]. Reproduced with permission from ref. [113]. Copyright 2018 American chemical society.

(Figure 9(b)), the authors suggested that these changes arise through guest-host-guest interactions induced by Li^+ exchange, which cause a reduction of the lattice parameter of zeolite and thus changed bond lengths of the Ag NCs (Figure 9(c)). Much efforts have been devoted to build the relationship between optical properties and structural parameters (such as the cluster size, geometry and charge) of these confined Ag NCs, which is similar to that of organic ligand protected NMNCs, but unexpectedly, the optical properties of these zeolite confined Ag NCs are closely related to their hydration state. In 2014, Lin et al. observed reversible emission evolution of Ag NCs in LTA zeolite upon dehydration/hydration in vacuum/water vapor [112], the yellow-green emission at 550 nm of these confined Ag NCs was quenched under vacuum conditions, accompanying with the enhancement of the red emission at 690 nm, and these changes were reversible when water vapor was added (Figure 10(a)). Based on these intriguing experiments, the authors suggested that origin of the emission from Ag activated zeolite may not be the quantum confinement effect of Ag NCs, but may be the charge transfer transition from the framework oxygen to Ag^+-Ag^0 with the participation of H_2O molecules. In the follow-up research work, the authors discovered that the emissions of the thermally-treated Ag^+ exchanged SOD zeolites were insensitive to the environmental change [116], in contrast to the notable reversible green/red dominant emission evolution of thermally-treated Ag^+ exchanged LTA zeolites. The difference is ascribed to the difficult H_2O permeation in SOD zeolites in comparison with LTA zeolites. Therefore the authors proposed the following emission mechanisms for thermally-treated Ag^+ exchanged LTA and SOD zeolites: the yellow-green emission is due to the transition from ligand-to-metal (framework $O_2^- \rightarrow Ag^+$) charge transfer (LMCT) state to the ground state and the red emission is due to the transition from the metal-metal (Ag^+-Ag^+) charge transfer (MMCT) state to the ground state, the hydrated water only distributed a shielding effect on neighboring Ag^+ ions, which could increase the distance between the neighboring Ag^+-Ag^+ ions and impede the formation of Ag_n^{m+} clusters, and thus the yellow-green emission at 550 nm observed for Ag NCs at hydration state was dominated by the mechanism of LMCT, while the red emission at 690 nm for Ag NCs at dehydration state was dominated by the mechanism of MMCT. Grandjean et al. also observed the remarkable reversible on-off photoluminescence switching of Ag NCs confined in LTA zeolite upon dehydration and rehydration [115], but it was demonstrated that the fully dehydration of the samples, confirmed by the absence

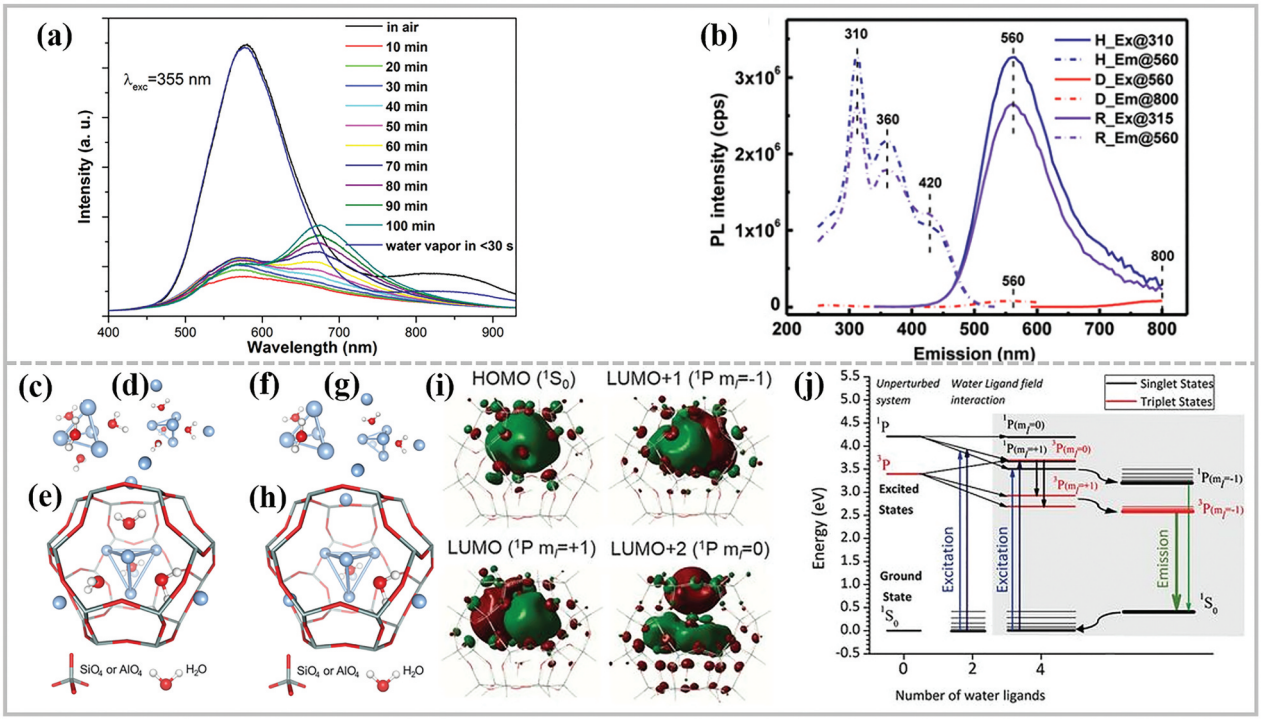

Figure 10. (a) PL evolution of $Ag_{4.4}$, $Na_{7.6}$-A from air to vacuum then to water vapor [112]. Reproduced with permission from ref. [112]. Copyright 2014 AIP Publishing LLC. American chemical society. (b) PL intensity of the sample at different excitation (Ex.) and emission (Em.) maxima in the hydrated (H), dehydrated (D) and rehydrated (R) state [115]. Reproduced with permission from ref. [115]. Copyright 2018 the Royal Society of Chemistry. (c to h) Structures of (c) $Ag_4(H_2O)_4$ and (f) $Ag_4(H_2O)_2$, including [(d) and (g)] Ag_R cations and [(e) and (h)] embedded in the sodalite cage (~0.66 nm free diameter). (i) Frontier orbitals of $[Ag_4(H_2O)_4(Si_{24}H_{24}O_{36})]^{2+}$ and (j) energy level diagram of $Ag_4(H_2O)_2^{2+}$ and $Ag_4(H_2O)_4^{2+}$ clusters in Ag_3K_9-LTA [6]. Reproduced with permission from ref. [6]. Copyright 2018 American association for the advancement of science.

of the water and hydroxyl vibrational bands in FTIR spectra, can be only achieved after a treatment up to 450 °C under vacuum (0.1 mbar pressure), and the fully dehydrated samples were almost non-luminescent but the green-yellowish emission at 560 nm was regenerated after rehydration of the dehydrated samples at room temperature (Figure 10(b)). The authors believed that water coordinated, diamagnetic, tetrahedral Ag clusters $[Ag_4(H_2O)_4]^{2+}$ with Ag atoms positioned along the axis of the sodalite six-membered rings are at the origin of the green-yellowish luminescence in the hydrated sample. Upon dehydration, luminescent $[Ag_4(H_2O)_4]^{2+}$ clusters are transformed into non-luminescent (dark), diamagnetic, octahedral Ag clusters $[Ag_6(O_F)_{14}]^{2+}$ with Ag atoms interacting strongly with zeolite framework oxygen (O_F) of the sodalite four-membered rings. Besides, by means of a combination of x-ray excited optical luminescence-extended x-ray absorption fine structure, time-dependent-density functional theory calculations, and time-resolved spectroscopy, the authors further elucidated that the optical properties of the $Ag_4(H_2O)_x^{2+}$ (x = 2 and x = 4) clusters (Figure 10(c-h)) originate from a confined two-electron superatom quantum system with hybridized Ag and water O orbitals delocalized over the cluster (Figure 10(i,j)) [6]. Upon excitation, one electron of the s-type highest occupied molecular orbital is promoted to the p-type lowest unoccupied molecular orbitals and relaxes through enhanced intersystem crossing into long-lived triplet states. In these cases, there is no doubt that hydrated water take a crucial role in tuning the luminescence properties of Ag NCs confined in zeolites, and the emission energy and pathways of these Ag NCs was highly dependent on their hydration degree. Whereas, the local environment of these confined Ag NCs was much more intricate due to the multiple host-guest interaction between zeolite and Ag NCs, by comparing with organic ligand-protected NMNCs, and the structure of the Ag NCs is also sensitive to the environment changes, the mechanism of the role of hydrated water needs more experimental and theoretical investigation. Besides, as water is ubiquitous in the solvent or air atmosphere, it is unavoidable that there is trace amount of water adsorbed on the organic ligand protected NMNCs. For instance, Perić et al. recently demonstrated that the water surrounding on the metal NCs core significantly influenced the PL properties of multi-shell zwitterion functionalized gold nanoclusters, which depended on the penetration depth of water molecules into NCs core [117]. The authors observed that more dense packing of surface protective ligands on the core produced the stronger PL emission by blocking the water diffusion on the metal core, and they pointed out that, the surrounding water molecules indeed played a quenching role for the PL emission of metal NCs. In fact, in our structure water model, the same quenching role of surrounding water on metal NCs PL emission was also observed, which is attributed to the destabilization effect of surrounding water on SWs due to hydrogen bonding interactions. Obviously, the surrounding water is hardly to influence the metal core state with defined compositions and geometry (Figure 3), suggesting the rationality of SWs as emitter center for PL emission. In the section 3, we will discuss this point in details.

3. PBIS model

As discussed above, both types of NMNCs have well-defined structure and composition [2,6,73,74], which mainly comprised by the metal core and ligand or ligand-metal complexes shell, and each components showed a significant effect on the PL properties of NMNCs. The size effect of metal core (quantum confined effect), the coordination interaction between ligand and metal (ligand-to-metal charge transfer transitions, LMCT and/or LMMCT) and the interaction between metal cations within ligand-metal complexes are all involved to understand the luminescence mechanism of NMNCs, whereas a unified understanding of luminescent NMNCs have not been achieved, the elucidation on the origin of the optoelectronic properties of NMNCs is still diverse and even contradictory [63]. Intriguingly, the interaction between ligand (including ubiquitous water molecules) bound or confined on the metal core at nano-interface or -space have been largely overlooked. Recently, in contrast to conventional metal-centered emission mechanism, we firstly attributed the unique optical properties of NMNCs to the strong electronic interaction between ligand bound on the confined metal core based on our continuous and long-term investigation on the nature of the PL of NMNCs [22,63,103,118–124]. A completely new p band intermediate state (PBIS) model, stemmed from the overlapping of *p* orbitals of the paired or more adjacent heteroatoms (O and S) of interfacial ligand through space interaction, was proposed to understand the nature of the bright PL of NMNCs. The interaction model within PBIS can be approximate described by the molecular orbital theory, in which both the spatial distance and orientation between adjacent heteroatoms of ligand showed a significant impact on the strength of PBIS. The PBIS model can well rationalize the abnormal optical phenomena reported in the literature. In this section, we describe the history of the PBIS model.

To fully understand the photoemission mechanism of NMNCs, the relationship between structure and optical properties of NMNCs must be firstly elucidated. In our earlier investigation, we separately investigated the contribution of the ligand shell and the metal core to understand the nature of photoluminescence of Ag NCs using carboxylate-protected silver

nanoclusters (Ag-carboxylate NCs) as a model [22]. Several crucial structural components were identified for achieving highly luminescent Ag NCs: (i) Highly fluorescent Ag NCs were synthesized using one-step aqueous photoreduction in the presence of multidentate ligands made of polyelectrolyte poly(methacrylic acid) (PMAA) anchoring groups. The absorption and PL intensity was positively related to the radiation time, suggesting the formation of metal core is conductive to construct the emission center for highly luminescent Ag NCs (Figure 11(a,b)). (ii) Diagnostic experiments, in which dosing Ag^+ and Cl^- resulted the increase and decrease in PL intensity respectively, suggested the indispensable role of Ag^+ in the construction of the emission center (Figure 11(c,d)). (iii) When the poly(methyl vinyl ether-alt-maleic acid) (PMVEM) with the same anchoring ligand as PMAA was used as the surface anchoring ligand, the wavelength of both absorption and luminescence was blue shifted (Figure 11(e,f)). Notably, when the surface anchoring ligands were replaced by poly-(sodium-4-styrenesulfonate) free of carboxylate groups, as-synthesized Ag NCs with similar particle size showed undetectable PL intensity. These results emphasized the vital role of ligands to regulate the PL properties of Ag NCs. Based on these experiment results, a Ag(0) NCs@Ag(I)-carboxylate complex core-shell structural model was proposed to understand the nature of photoluminescence of Ag NCs (Figure 11(g)). We concluded that the origin of photoluminescence from Ag NCs cannot be simply attributed to the quantum confined effect (discrete Fermi energy levels) in the Ag NCs but highly dependent on the ligand-to-metal-metal charge transfer (LMMCT) from Ag(I)-carboxylate complexes to the Ag atoms. However, how the surface ligand regulated the optical properties of NMNCs is still unclear at this stage.

Followed the above research, in the aqueous solution, both Ag NCs synthesized using PMVEM and PMAA as templates (labeled as PMVEM-Ag NCs and PMAA-Ag NCs respectively) exhibited a fluorescence with low quantum yield (QY ≈ 1.0%) and short lifetime (τ ≈ 1.0 ns). Whereas, in the dimethyl sulfoxide (DMSO) solution, these water-soluble Ag NCs suffered aggregation due to the hydrogen-bond breaking capacity of DMSO, and the optical properties of these aggregated Ag NCs was highly dependent on the nature of surface ligand [118], the PMVEM-Ag NCs exhibited the fluorescence-phosphorescence dual solvoluminescence including a short-wavelength emission at ~460 nm with a short lifetime of 1.6 ns, which is same as the one in water, and a new generated long-wavelength emission at ~530 nm with a remarkably long lifetime of 97.1 μs and high QY of 40% (Figure 12(a-d)). Whereas, no phosphorescence was observed for PMAA-Ag NCs in

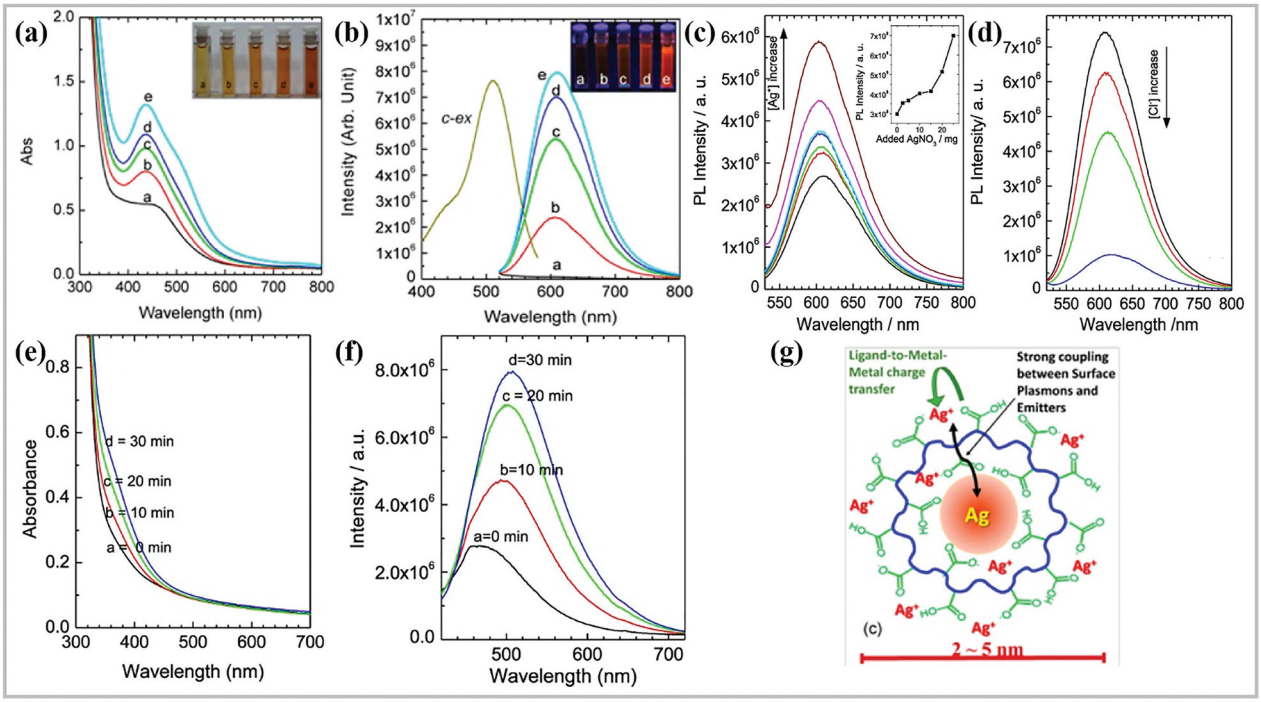

Figure 11. (a) UV-vis absorption and (b) photoemission spectra of the freshly prepared Ag-carboxylate NCs using PMAA as scaffold at various radiation times (a, 0 min; b, 10 min; c, 20 min; d, 30 min; and e, 40 min.). Inset images show the corresponding photographs of Ag-carboxylate NCs under room and UV light exposure at λ = 365 nm. Luminescence enhancement and quenching by addition of (c) Ag^+ and (d) Cl^- into the aqueous Ag-carboxylate NC solutions. Inset in (c) displays the relationship between PL intensity and added $AgNO_3$. (e) UV-vis absorption and (f) photoemission spectra of Ag NCs prepared with PMVEM scaffold under UV photoreduction. (g) Schematic illustration of the structures of our luminescent Ag-carboxylate with Ag^+-carboxylate complexes shell [22]. Reproduced with permission from ref. [22]. Copyright 2014 American chemical society.

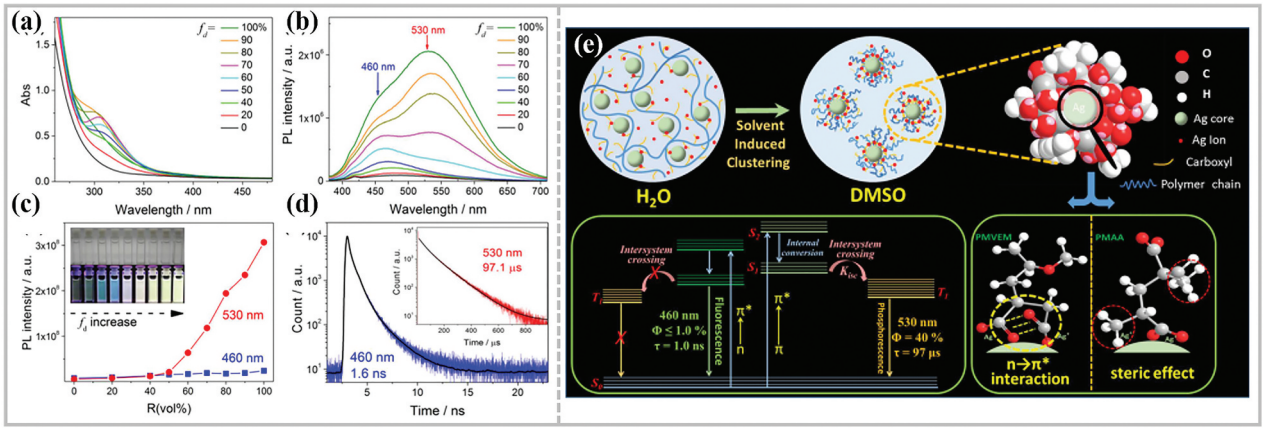

Figure 12. (a) UV-vis absorption and (b) photoluminescence spectra of PMVEM-Ag NCs in the varied volume fraction f_d of DMSO in the mixed solvent ($f_d = V_{DMSO}/V_{DMSO+water}$). (c) Correlations of the emission intensities of the two peaks centered at ~460 and ~530 nm versus f_d. (Inset) Photographs of PMVEM-Ag NCs at different f_d under visible (top row) and UV (bottom row) light. (d) Time-resolved luminescence decay profiles of PMVEM-Ag NCs in DMSO measured at 460 and 530 nm (inset), respectively. (e) Schematic illustration of the solvent-induced clustering process of Ag NCs (top) depending on the unique molecular structure of the polymer used as a template for the synthesis of Ag NCs (bottom-right) and the energy-level structure of Ag NCs in water solution and DMSO solution (bottom-left) [118]. Reproduced with permission from ref. [118]. Copyright 2017 American chemical society.

the DMSO solution. Although both the polymer templates bear abundant carboxylate groups on the flexible carbon chain, the difference in the conformation of carbonyl groups resulted the difference in optical properties of Ag NCs at aggregation state. The phosphorescence of PMVEM-Ag NCs was attributed to the aggregation of surface carboxylate ligands on the metal core, that is, the cluster formation of carbonyl groups, the efficient delocalization of electrons in overlapped C=O double bonds between neighboring carbonyl groups triggered by strong n → π* interactions in the polymer cluster formed an exact chromophore of metal NCs for AIE mechanics. However, the conjugation or delocalization of electrons between carbonyl groups cannot occur in the PMAA-Ag NCs due to the steric effect of methyl groups connected to the proximal carbonyl group of the polymer chain (Figure 12(e)). The mechanism highlighted the strong interaction between surface ligand rather than the metallophilic interaction on the metal NC center within AIE mechanics.

Based on the above mechanism, the optical properties of NMNCs should be strongly dependent on the binding group and assembly model of surface ligand on metal core. In the following research, by manipulating the delicate surface ligand interactions at the nanoscale interface of a single metal nanocluster, the superlattice, and mesoporous materials, we isolated the role of the local patterning or spatial arrangement of surface ligands in the PL emissions of metal NCs, the photoemission of Au NCs was more sensitive to the type and the assembly of surface ligand rather than the size of metal core and the type of metal [120], as shown in Figure 13, water-soluble Au NCs protected by glutathione (Au NCs@GSH) bearing both carbonyl and thiol group exhibited a broad emission peak at ~560 nm with a long lifetime of 14.6 μs in the ethanol solution, showing a strong solvent-enhanced PL emission behavior (Figure 13(a,d)). The broad emission can be decomposed into two peaks located at 550 and 620 nm using Lorentzian functions, whereas, when the hydrophilic GSH ligand of Au NCs was replaced by 1-dodecanethiol (Au NCs@DT) with a single thiol group through a simple surface ligand exchange reaction, as-obtained oil-soluble Au NCs exhibited a sharp emission peak at ~620 nm with a long lifetime of 3.7 μs in the aqueous solution (Figure 13(c,d)), as Ag NCs protected by PMVEM with single carbonyl group exhibited a similar phosphorescence with the emission peak at 530 nm [118], we hypothesized that the two emission peaks at 550 and 620 nm of water soluble Au NCs@GSH was the consequence of the clustering of carbonyl and thiol group respectively due to the solvent-induced aggregation. Furthermore, except for Au NCs@DT, Cu NCs protected by DT (Cu NCs@DT) ligand can assembly different superlattices (nanoribbon and nanosheet), which exhibited different emission color, Whereas, when breaking the superlattices into isolated Cu NCs by ultrasonic treatment, the PL of superlattices was quenched, but when these isolated and hydrophobic Cu NCs redispersed in the water, the Cu NCs@DT exhibited a red emission at 620 nm (Figure 13(e)), which is identical to that of Au NCs@DT. These results further supported the hypothesis, that means the clustering of the function group (-COOH/-SH) bearing on the targeting ligands could generate an intermediate state to activate the radiative transition of triplet state, we defined the intermediate state as PBIS, resulting from the strong overlapping of

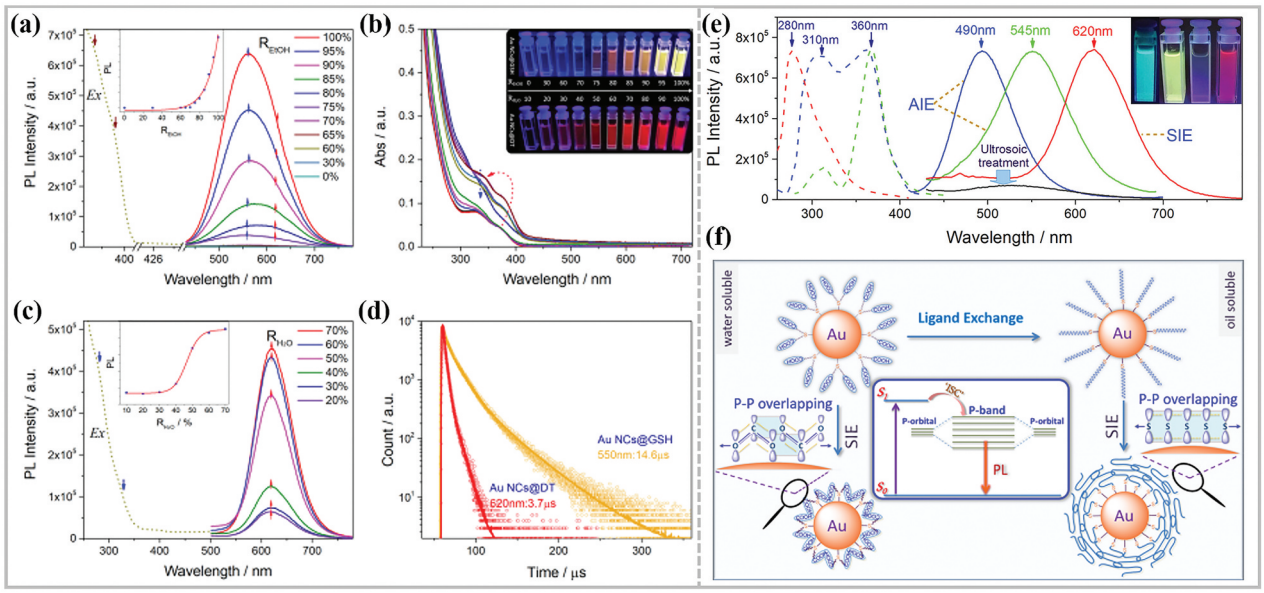

Figure 13. Photoemission and excitation spectra of water-soluble Au NCs@GSH (a) and oil-soluble Au NCs@DT (c) in mixed solvents with different volume fraction R (Inset, relationship between the luminescence intensity and R ($R_{EtOH} = Vol_{EtOH}/Vol_{EtOH+H2O}$, $R_{H2O} = Vol_{H2O}/Vol_{EtOH+H2O}$). (b) UV-vis absorption spectra of Au NCs@GSH in mixed solvents with different R_{EtOH}. Inset shows the digital photos of water-soluble Au NCs@GSH and oil-soluble Au NCs@DT in mixed solvents of ethanol and water with varied volume fraction R_{EtOH} and R_{H2O} under UV light. (d) Time-resolved luminescence decay profiles of solvent-induced luminescent Au NCs@GSH and Au NCs@DT. (e) Excitation (dash) and emission spectra of Cu NCs SL with nanoribbon structure (blue), nanosheet structure (green), and individual Cu NCs in water (red). The insert shows the corresponding digital photos under UV light. AIE stands for the assembling-induced emission of the SL, and SIE is solvent-induced emission for individual metal NCs in a poor solvent. (f) Schematic illustration of the ligand exchange process and solvent-induced emission (SIE) properties of Au NCs (inset: the energy-level structure of Au NCs in water and ethanol mixed solution). The p-band formed by the overlapping of p-orbitals of electron-rich sulfur and oxygen heteroatoms of well-organized surface ligands is used as an intermediate state or dark state to tune the optoelectronic properties [120].

p orbitals of the heteroatoms (O, N, and S) bearing on the targeting ligands though space interactions (Figure 13(f)). Differed in the metal-centered free-electron model, the PBIS model give a totally new insight to understand the nature of the PL of NMNCs and other low other quantum dot systems. More importantly, based on the concept of PBIS model, we successfully construct the chromophore by the assembly of ligand in the confined mesopores of mesoporous silica nanoparticles (MSNs) through functionalized by non-luminescent organosilanes with amino and carbonyl groups free of any metals (Figure 14), the amino-functionalized and carbonyl-functionalized MSNs exhibited a blue emission at 430 nm and a red emission at 615 nm, respectively (Figure 14(c,d)). Both the nano-sized metal core of NMNCs and mesopores of MSNs imposed a strong space interaction on the adjacent p orbitals of the heteroatoms (O, N, and S) bearing on the ligands, which is conductive to the formation of PBIS. The concept of PBIS can rationalize these abnormal PL phenomena, however, the physical-chemical nature of PBIS is still unclear. Further investigation on the optical properties of inorganic scaffold confined NMNCs give us some new inspiration on the nature of PBIS [123]. Luminescent Ag NCs confined in the LTA zeolite (Ag NCs@LTA) was readily prepared through a cation-exchange and a thermal reduction process. The Ag NCs confined in the zeolite was highly hydrated, in which the water acts the role of ligand, thus it is rational that the optical properties of Ag NCs was strongly dependent on the hydration state based on the PBIS model. The hydration degree of Ag NCs@LTA can be tuned through thermal treatment or dispersing in different solvents (Figure 15(a-d)), fully hydrated Ag NCs@LTA at room temperature or dispersed in water exhibited a broad emission peak at 525 nm with a short lifetime of 3 ns, whereas, partially hydrated Ag NCs@LTA after thermal treatment at 250 °C or dispersed in DMSO exhibited a red emission peak at 605 nm with a long lifetime of 231.1 us (Figure 15(a,d)), and fully dehydrated Ag NCs@LTA was non-luminescent as introduced in the section 2. Besides, the PL intensity of hydrated Ag NCs@LTA was gradually decreased with increasing time of vacuumizing but increased when replacing solvent water (H_2O) by heavy water (D_2O) accompanying with a sight red-shift in emission wavelength (Figure 15(e,f)). Notably, without any noble metal, NH_4^+ exchanged zeolite Y also exhibited a blue emission at 430 nm after thermal treatment at 200 °C (Figure 15(g)), and the blue photoemission was ultra-stable at liquid nitrogen temperature with an ultra-long lifetime up to second scale (Figure 15(h)).

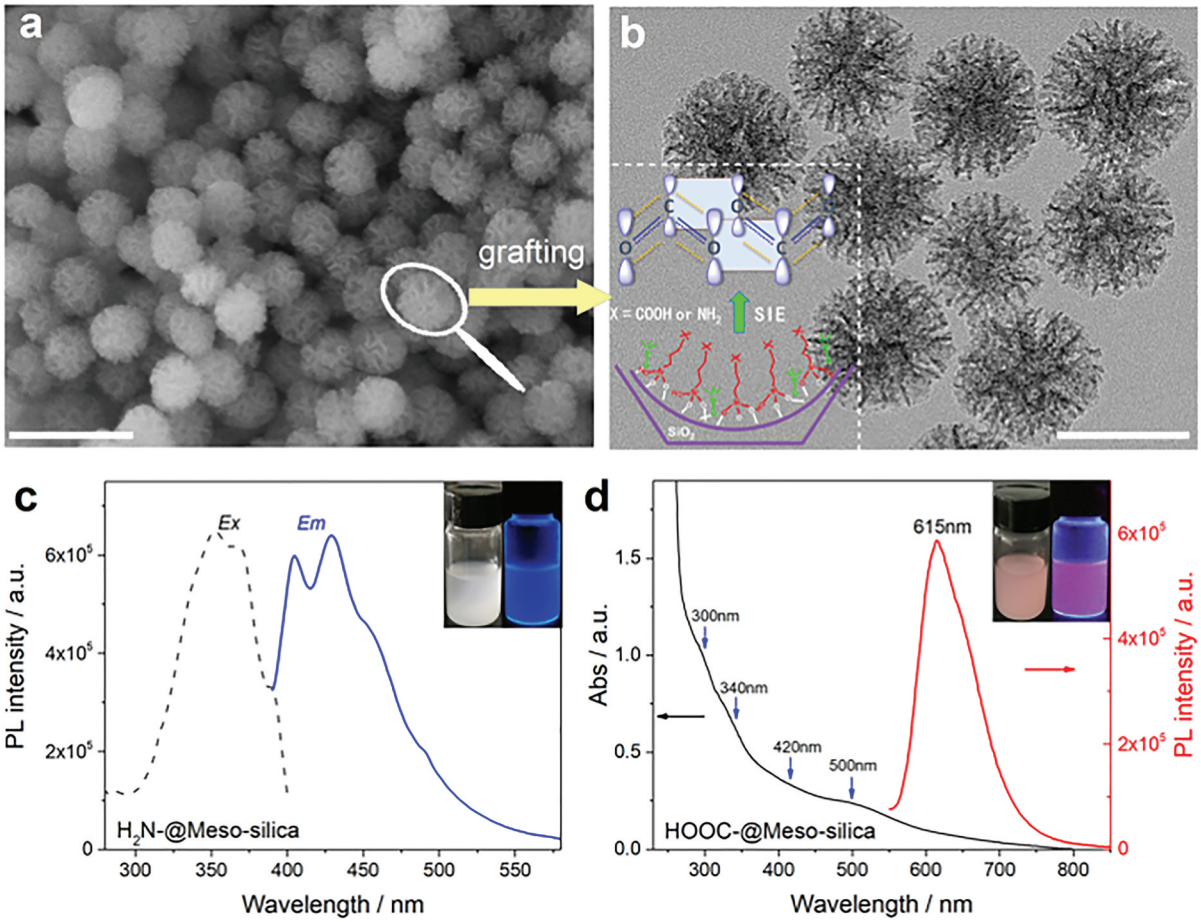

Figure 14. Scanning electron microscopy (SEM) (a) and TEM (b) images of as-synthesized fluorescent mesoporous silica nanoparticles. The inset shows the assembly of amino- and carbonyl- groups in the confined nanopores. (The scale bar in a and b is 200 and 100 nm, respectively.) (c) Excitation and emission spectra of aminopropyl-functionalized MSNs. (d) Absorption and emission spectra of propylsuccinic-functionalized MSNs [120].

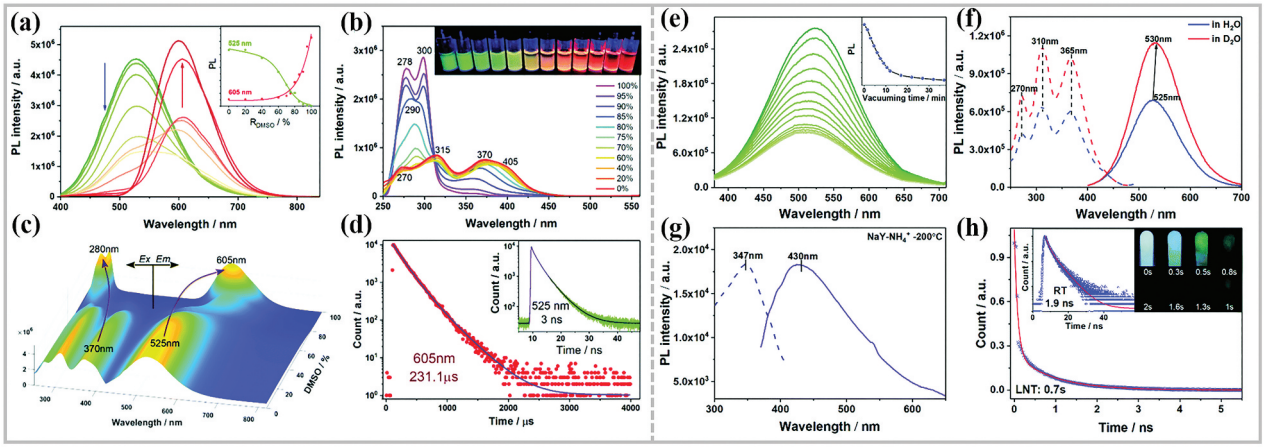

Figure 15. (a) Photoemission and (b) UV-vis absorption spectra of Ag@LTA-450°C in the varied volume fraction of DMSO in the mixed solvent ($f_d = V_{DMSO}/V_{DMSO+water}$). (c) Contour representation of the excitation and emission data with varied f_d for Ag@LTA-450°C. (d) Time-resolved luminescence decay profiles of Ag@LTA-450°C in water (green) and DMSO (red) solution. (e) PL decrement of hydrated Ag@LTA-450°C with increasing time of vacuumizing. The inset shows the corresponding PL intensity attenuation (at 525 nm) during the dehydration process. (f) Comparison of emission properties of Ag@LTA-450°C in H_2O and D_2O. (g) Excitation (dashed line) and emission spectra (solid line) of NH_4^+-Y-type zeolite annealed at 200°C. (h) Time-resolved luminescence decay profiles of NH_4^+-Y-type zeolite at room temperature (RT) and liquid nitrogen temperature (LNT). Inset shows the naked eye visible long afterglow emission at LNT [123]. Reproduced with permission from ref. [123]. Copyright 2021 the Royal Society of Chemistry.

The PL of Ag NCs@LTA was therefore attributed to the formation of hydrated hydroxide complex $OH^-{\cdot}H_2O$ (defined as SWs) in the confined nanocavity beyond PBIS mechanism, but a critical question is that what is the physical nature or chemical principle for the formation of PBIS. For instance, hydrogen-bonded water is a colorless liquid, it is confusing that the interfacial water bound to the NMNCs or confined in the nanopores can emit bright color. Therefore, it is important to elucidate the difference in chemical nature between hydrogen bonded water and interfacial water with photoemission. Free water molecules firstly formed an adsorption bond between oxygen atom and interfacial sites X (X could be Ag^+ ions, alkali metal ions, and protons), subsequently, the nano-sized metal NCs or micropores of zeolite imposed strong space interaction on these adjacent adsorption bond, which could induce the re-distribution of the localized chemical bonds on the molecule level (Figure 16). The formation of PBIS could be described as a result of a linear combination of extended sp hybrid orbitals between O p orbitals and X s orbitals based on the principle of molecular orbital (MO) theory. The derived PBIS contained a π^* state with π bond character due to the overlapping of p orbitals of oxygen atoms, which can account for the physical origin of the PL of SWs, and a σ^* state with a σ bond character due to the overlapping of s orbitals of X, which could give a new fundamental understanding on the origin of metallophilic interactions between the closed-shell metal centers. Besides, combined with time-resolved steady state and ultra-fast femtosecond (fs) transient optical spectroscopy, a scenario of deactivation involving the energy delocalized excitation producing an ensemble of states (Q_n and Q'_n) with mutually different polarizations that decay via multiple channels was represented in Figure 16(c). The observed multiple sets of quantum transient states (Q_n and Q'_n) are concurrently produced, and the main optical absorption and emission are extremely susceptible to delicate change of microenvironments surrounding the emitter center. Therefore, the effect of metal core (size, composition, valence state, *etc.*), ligand shell (type, architecture, *etc.*) and external stimulus (pH, solvent, temperature, ions, *etc.*) on the optical properties of NMNCs can be rationalized by the chemical nature of PBIS which followed the bonding principle of molecular orbital theory. For instance, the negative influence of the PMMA on the PL emission efficiency of Ag NCs in our earlier investigation can be easily understood since the adsorbed content and the acting mode of structural water on the Ag NCs core are changed owing to the hydrophobicity of methyl groups bearing on the PMMA [118]. Besides, the fundamentals of PBIS mechanisms could give a unified interpret for the luminescence properties in the community of

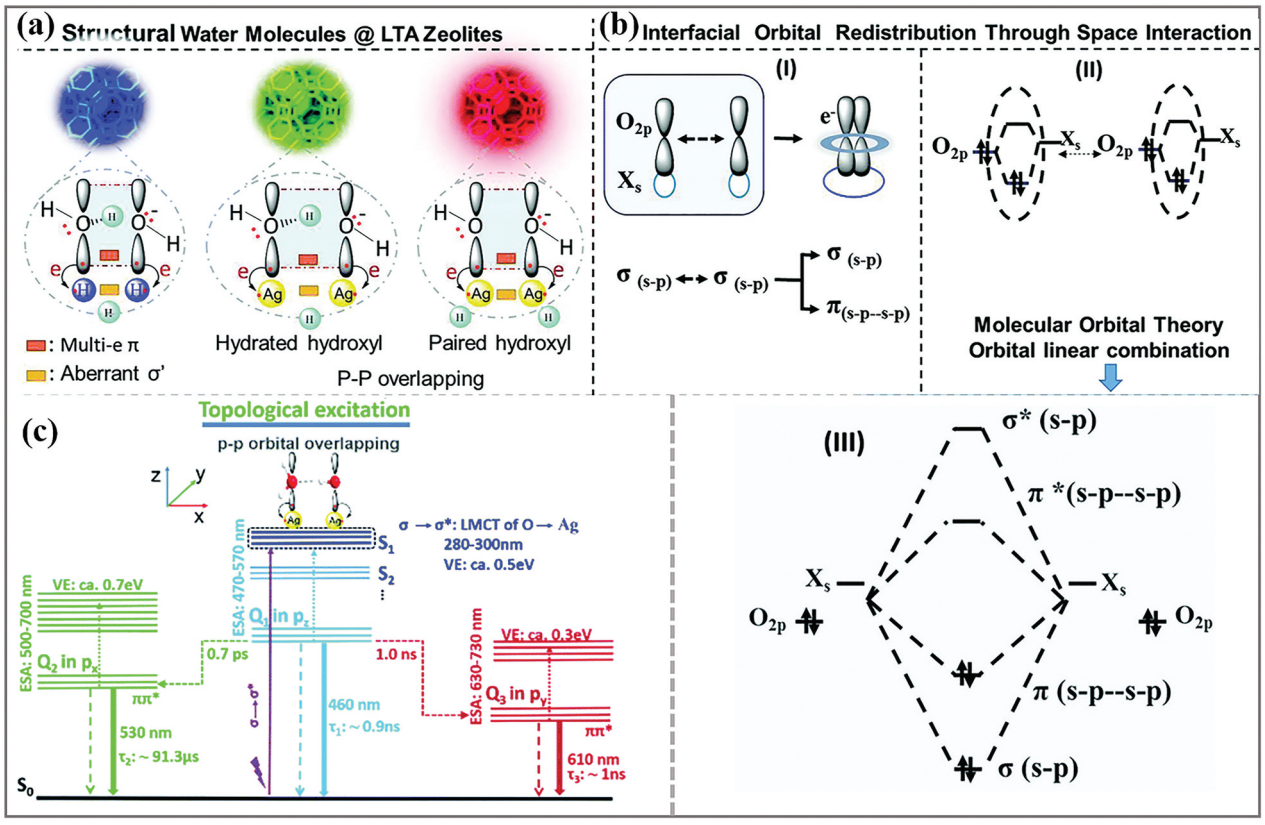

Figure 16. Schematic illustration of the interfacial orbital redistribution through space interactions induced bright and wavelength adjustable photoluminescence of Ag@LTA and corresponding energy level structure derived from molecular orbital theory [123]. Reproduced with permission from ref. [123]. Copyright 2021 the royal society of chemistry.

ligand protected metal NCs and also answer the century debate about whether and how adsorbed water can emit bright colors [125,126].

The luminescence of SWs in the system Ag NCs@LTA inspired us to revisit the nature of the PL of ligand protected NMNCs as water is ubiquitous in the natural world, and the formation of PBIS between SWs is more available than that between organic ligands which could show a large steric effect on the overlapping of p orbitals of the heteroatoms (O, N, and S) bearing on the ligands. In the following research, the silver cations were introduced into the oil-soluble Au NCs@DT, the obtained Ag-Au bimetallic NCs exhibited an interesting silver cation-mediated dual-emission behavior, in which the blue emission at 440 nm with a lifetime of 5.4 ns is arouse by the doping of silver and the red emission at 620 nm with a lifetime of 2.0 us is the same as the PL of monometallic Au NCs@DT (Figure 17(a-d)) [122]. Furthermore, the dual emission of Ag-NCs was highly pH-dependent in the ethanol solution, in which the red emission dramatically reduced and almost quenched while the blue emission increased two times after dosing NaOH in the solution (Figure 17 (e,f)), the variation in pH of the solution can hardly affect the assembly of the nonionic alkylthiol (DT) ligands but show a significant effect on the interfacial water, therefore, it is more rational to attribute the PL of Ag-Au bimetallic NCs to the formation of PBIS between unconspicuous interfacial water molecules adsorbed on the metal sites (Figure 17(g-j)). This again answers that, why the PL properties of monolayer protected clusters and metal-thiolates complexes are extremely sensitive to the composition of metal NCs, the type of surface protective ligand and even the surface ligand packing mode or assembly [22,118–120,127]. Very recently, some of us demonstrated that [127], just by manipulating noncovalent interactions of the ligand-ligand and ligand-metal interactions, the silver-glutathione (Ag(I)-GSH) supramolecular assemblies could be readily synthesized with blue and orange color, and interestingly that their color can be reversibly tuned, and exhibited a 4 orders of magnitude variation in fluorescence lifetime and dramatically different excited state dynamics. In addition, using PBIS dominated structural water model, the surface-ligand coverage dependent and non-size-dependent PL emission of GSH protected Au NCs can be easily understood: at high (or dense) ligand coverage, due to the limited number of adsorbed of water, the short-range conjugation of *p* orbitals of O atoms leads to the high energy emission at 600 nm, while at low coverage of surface protective ligands of GSH, more water molecules are adsorbed on

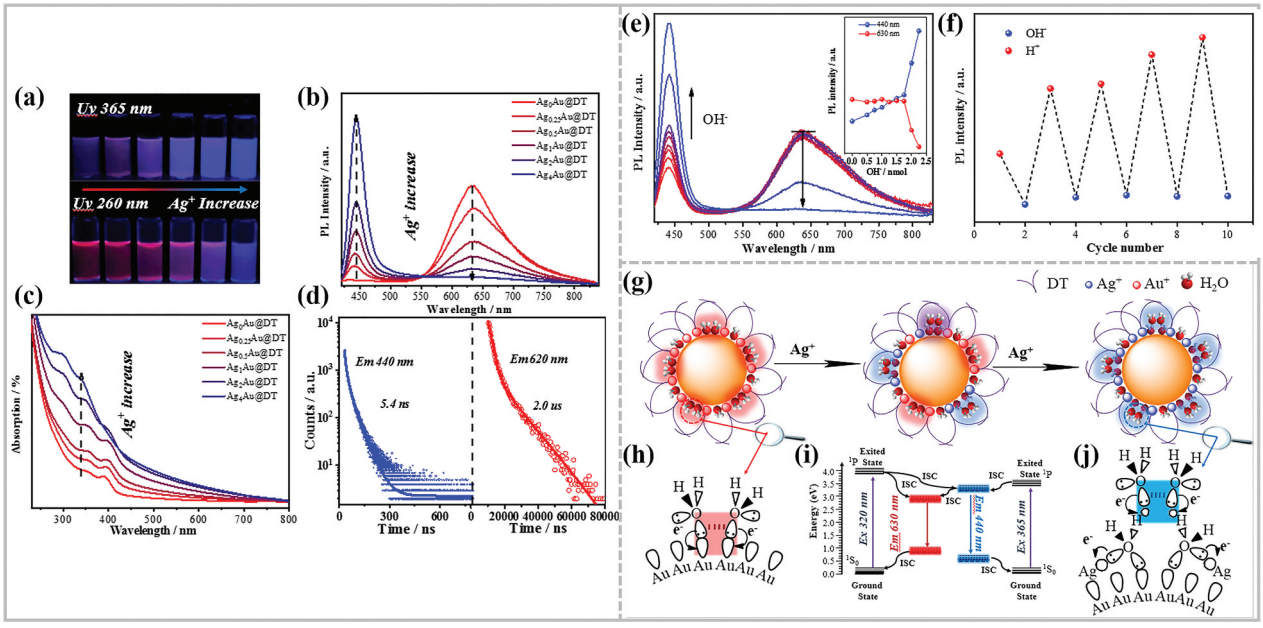

Figure 17. (a) Luminescent photographs of Ag_xAu@DT NCs under UV 365 nm (top) and 260 nm (bottom) irradiations. (b) Photoemission spectra and (c) absorption spectra of Ag_xAu@DT NCs. (d) Time-resolved luminescence decay profiles of Ag_1Au@DT NCs measured at 440 nm (left) and 630 nm (right), respectively. (e) Photoemission spectra of as-synthesized Ag_1Au@DT NCs after adding increasing amounts of 50 mM NaOH aqueous solution. The inset displays the relationship between PL intensity and the added mole amount of NaOH. (f) PL intensity of Ag1Au@DT NCs upon cyclic switching of the pH by adding 50 uL 50 mM NaOH and 50 uL 50 mM HCl aqueous solution. (g) Schematic illustration of structural water molecules (SWs) confined at nanoscale interface of Au-Ag bimetal NCs packed by protective ligands emit bright dual-photoluminescence, (h) the red emissive SWs strongly binding on the single metal Au NCs, (j) the blue emissive SWs weakly binding on the fully core-shell structured Au-Ag bimetal Au NCs though water bridge which strongly coordinated with Ag^+ and (i) energy diagram of dual emissions of Au-Ag bimetal NCs [122].

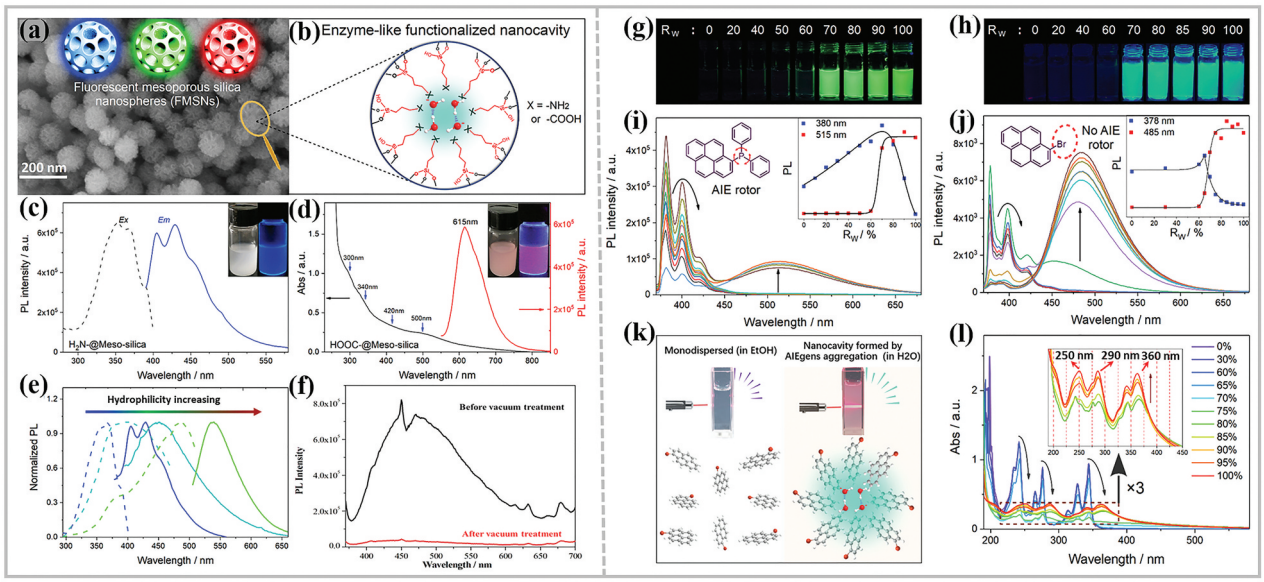

Figure 18. (a) SEM images of as-synthesized fluorescent mesoporous silica nanoparticles (FMSNs). (b) the formation of SWs in an amino and carbonyl-group-functionalized enzyme-like nanocavity. (c) Excitation and emission spectra of amino-functionalized FMSNs. (d) Absorption and emission spectra of propylsuccinic-functionalized FMSNs. (e) Emission wavelength regulation of FMSNs by controlling the hydrophobicity of the nanopores. (f) Evolution of PL emission intensity of amino-functionalized FMSNs at ca. 450 nm by vacuum dehydration treatment. (g, h) Photographs and (i, j) fluorescence spectra of diphenyl-1-pyrenylphosphine (g, i) and 1-bromopyrene (h, j) in mixed solvents with different volume fractions R_w ($R_w = Vol_w/Vol_{e+w}$, the subscripts w and e represent water and ethanol, respectively). Inset shows the relationship between the luminescence intensity and R_w. (k) Proposed mechanism for water-induced AIE phenomenon. (l) Ultraviolet-visible (UV-vis) absorption spectra of 1-bromopyrene (BP) in mixed solvents with different R_w [103].

the metal core surface, the long-range conjugation of *p* orbitals of O atoms results in the low energy PL emission at 810 nm [53].

Followed this mechanism, we also re-investigated the nature of the PL of luminescent MSNs functionalized by non-luminescent organosilanes (Figure 18 (a-f)) [103]. The emission wavelength of amino-functionalized MSNs was blue-shift with the increase in the grafting amount of hydrophobic functional groups (trimethyl chlorosilane) within the mesopores (Figure 18(e)). More prominently, the PL of amino-functionalized MSNs was almost quenched after vacuum treatment (Figure 18(h)), that means the SWs was the true emitter for the luminescent MSNs and the amino group took a similar role of metal in the NMNCs for the adsorption of water. Similarly, the conceptual of confined SWs as a bright emitter is also possible to account for the AIE effect which is both observed for conjugated and non-conjugated organic molecules and metal-thiolate complexes. The nature of AIE is indeed a solvent driven molecular self-assembly process, the aggregation of AIE luminogens (AIEgens), such as typical AIEgens of diphenyl-1-pyrenylphosphine (DPPP, Figure 18(g,i)) and classical organic chromophores (1-bromopyrene, BP, Figure 18(h,j)) trigged by the introducing of bad solvents could also possibly construct a soft nanocavity for the formation of SWs emitters (Figure 18(k)), which is analogous to the rigid nanocavity (mesopores) in luminescent MSNs (Figure 18(b)). Therefore, in some of case, the AIE effect is not sensitive to the structure of AIEgens, the classical mechanism of restriction of intramolecular motions (RIM) was still working during the aggregation process, but the PL may not be originated from the AIEgens itself but the SWs confined in the soft nanocavity constructed by the AIEgens.

4. Summary and outlook

In this mini-review, we firstly summarized recent advances in the PL mechanism of NMNCs, several prevailing PL mechanisms, including quantum confinement effect (QCE), ligand to metal charge transfer (LMCT) or ligand to metal-metal charge transfer (LMMCT) and metallophilic interaction beyond AIE effect, *etc.*, were involved in explaining the effect of structural components (metal core, organic ligand shell and interfacial water), local environments and external stimulus (pH, solvent, ions, *etc.*) of NMNCs on their PL properties, but there is still no basic consensus on the elucidation of the PL mechanism of NMNCs. Then, we revisited our studies on the PL mechanism of NMNCs, a completely new PBIS model, stemmed from the overlapping of *p* orbitals of the paired or more adjacent heteroatoms of interfacial ligand (especially emphasized the oxygen atom of SWs) through space interaction, was proposed to understand the nature of the bright PL of NMNCs. Note

that water in the term of SWs does not distinguish between the three possible protonation states, water/hydroxo/oxo, which is extremely sensitive to the surrounding microenvironment of SWs at confined nanoscale interface. By combining the literature survey and our long-term studies in the past decade, we draw the conclusion that SWs dominated PBIS model can well rationalize the abnormal optical phenomena reported in the literature and give a unified understanding on the PL mechanism of NMNCs.

Based on the fundamentals of the SWs dominated PBIS model, not only the optical properties of NMNCs, we believe that it can be also extended to understand other unique properties (such as catalysis, chirality, *etc.*) of NMNCs. For instance, strong Cotton effects (circular dichroism, CD) of NMNCs protected by chiral ligands have been reported a long time ago [40,43], *e.g.* the in-situ-formed Ag(I)-thiolate polymers upon mixing $AgNO_3$ and chiral ligand (cysteine) exhibited intense absorption and CD signals in the range 200–400 nm, which affords signal amplification for cysteine sensing [45], whereas, the absorption characteristics of the chiral Ag(I)-thiolate polymers were almost identical to that of Au(I)-thiolate polymer using achiral dodecanethiol as ligand reported in our recent research work [121,122], which have been, herein, ascribed to the formation of PBIS within SWs on the NMNCs, that means the new-formed CD signals of these NMNCs can be also well rationalized by the SWs dominated PBIS model.

Furthermore, the principle for the formation of PBIS within SWs was also analogous to that for the formation of transition state between reactant molecules, NMNCs, which provided confined interface and/or space, can largely reduce the potential barrier for the formation of strong intermolecular interaction (interfacial state or transient state), which favored the formation of PBIS within SWs for bright PL, or favored the formation of metastable transient state between reactants for fast reaction kinetics [103,128–133]. Within this scenario, these unique properties of NMNCs can be well elucidated, and therefore the rational design of metal NCs with excellent optical and catalytic properties can be guided although much work remains to be done, even beyond the often used noble metal NCs (Au/Ag/Cu/Pt), such as transition metals and transition metal oxides [134–136]. Herein, in particular at basic conditions (pH > 7.0), we take hydrogen evolution reaction (HER) as a typical example to show the key role of SWs as reaction center to enhance reaction kinetics [132]. With Co-C-N as an prototype electrocatalyst, the reaction dynamics of HER does not follow the classical two-step process of Volmer step and Heyrovsky step (or Tafel step), while working the p band mediated electron transfer process for the direct activation of O-H bonds of water: the dissociated H^+ from water don't need to adsorb on the metal active sites, where SWs adsorbed on metal cations can directly interact with the water reactants, owing to the space interaction of p orbitals in SWs and water reactants, the energy level of the formed p band anti-bonding level (π^*) is even higher than that of the σ anti-bonding (σ^*) of O-H bonds in water, thus the electron can be directly fill with σ^* energy level, resulting in the O-H bond activation and hydrogen evolution [132,137]. Therefore, the p-band model proposed by us not only provides a new insight into the origin of PL emission of metal NCs, but also reveals the physical essence of interface (or surface) states at nanoscale interface for heterogeneous catalysis. On the one hand, the p-band accelerates the surface electron transfer through surface delocalization (or conjugation), and on the other hand, stabilizes the transition state of the chemical reaction.

Finally, from the perspective of the common nature of nanomaterials surface usually covered by water molecules [138,139], this significant conceptual advance of SWs model as emitters can be readily extended to understand the optical and catalytic properties of other quantum dot systems, including carbon and graphene nanodots [140–144], semiconductor quantum nanostructures [145–152], and, also provides a new insight into the PL emission mechanism of green fluorescent protein (GFP) [153–163].

Acknowledgments

K.Z. thanks ENS de Lyon for a temporary position as an invited professor in France. We are particularly grateful to Professor Fabien Grasset, as the invited editor, for inviting us to contribute a review article to the **STAM** Focus Issue on "*Metal Atom Clusters and Superatoms: From Fundamentals to Functional Nanocomposites*".

Disclosure statement

No potential conflict of interest was reported by the author(s).

Funding

This research was funded by the National Science Foundation of China [22172051, 21872053, and 21573074], the National Key R&D Program of China [2021YFA1501401], the Research Funds of Happiness Flower ECNU [2020ST2203], the Open Project Program of

Academician and Expert Workstation, Shanghai Curui Low-Carbon Energy Technology Co., Ltd., and the JORISS program.

Notes on contributors

Bo Peng, born in Yichun (Jiangxi Province, China), is currently a postdoctoral researcher at the College of Chemistry and Molecular Engineering of East China Normal University (ECNU, China) working with Prof. Kun Zhang and Prof. Ming-Yuan He. He received his B.S. (2017) from Donghua University (DHU, China) and Ph.D. (2022) from East China Normal University (ECNU, China). His research interests are mainly focused on the mechanistic understanding on the unique properties (photoluminescence, catalytic properties and chirality) of nanomaterials and therefore rational design of high efficient nanocatalysts towards the activation of small molecules (water and carbon dioxide) related to energy conversion。

Kun Zhang, born in Gaomi (Shandong Province, China), is currently a full Professor at the College of Chemistry and Molecular Engineering of East China Normal University (ECNU, China). In 2008, He received a Ph.D. in the Chemistry Laboratory at Ecole Normale Supérieure de Lyon (ENS-Lyon, France) working with Prof. Laurent Bonneviot and Prof. Ming-Yuan He. His research interests are mainly focused on the design of bio-inspired nanocatalysts towards the activation of small molecules related to energy conversion, such as water, methane (CH_4), carbon dioxide (CO_2), carbon monoxide (CO), oxygen (O_2), hydrogen (H_2) and nitrogen (N_2).

ORCID

Kun Zhang http://orcid.org/0000-0001-8418-1424

References

[1] Feynman RP There's plenty of room at the bottom. Annual Meeting of the American Physical Society, California; 1959 Dec 29; 1959.
[2] Jadzinsky PD, Calero G, Ackerson CJ, et al. Structure of a thiol monolayer–protected gold nanoparticle at 1.1 Å resolution. Science. 2007;318:430–433.
[3] Jin R, Zeng C, Zhou M, et al. Atomically precise colloidal metal nanoclusters and nanoparticles: fundamentals and opportunities. Chem Rev. 2016;116:10346–10413.
[4] Chakraborty I, Pradeep T. Atomically precise clusters of noble metals: emerging link between atoms and nanoparticles. Chem Rev. 2017;117:8208–8271.
[5] Yu H, Rao B, Jiang W, et al. The photoluminescent metal nanoclusters with atomic precision. Coord Chem Rev. 2019;378:595–617.
[6] Grandjean D, Coutiño-Gonzalez E, Cuong NT, et al. Origin of the bright photoluminescence of few-atom silver clusters confined in LTA zeolites. Science. 2018;361:686–690.
[7] Bodiuzzaman M, Dar WA, Pradeep T. Cocrystals of atomically precise noble metal nanoclusters. Small. 2020;17:2003981.
[8] Schaaff TG, Shafigullin MN, Khoury JT, et al. Isolation of smaller nanocrystal au molecules: robust quantum effects in optical spectra. J Phys Chem B. 1997;101:7885–7891.
[9] Lee D, Donkers RL, Wang G, et al. Electrochemistry and optical absorbance and luminescence of molecule-like Au38 nanoparticles. J Am Chem Soc. 2004;126:6193–6199.
[10] Negishi Y, Nobusada K, Tsukuda T. Glutathione-protected gold clusters revisited: bridging the gap between gold(I)-thiolate complexes and thiolate-protected gold nanocrystals. J Am Chem Soc. 2005;127:5261–5270.
[11] Walter M, Akola J, Lopez-Acevedo O, et al. A unified view of ligand-protected gold clusters as superatom complexes. Proc Natl Acad Sci USA. 2008; 105:9157–9162.
[12] Zhu M, Aikens CM, Hollander FJ, et al. Correlating the crystal structure of a thiol-protected Au25 cluster and optical properties. J Am Chem Soc. 2008;130:5883–5885.
[13] Bellina B, Compagnon I, Bertorelle F, et al. Structural and optical properties of isolated noble metal–glutathione complexes: insight into the chemistry of liganded nanoclusters. J Phys Chem C. 2011;115:245 49–24554.
[14] Zheng J, Zhang C, Dickson RM. Highly fluorescent, water-soluble, size-tunable gold quantum dots. Phys Rev Lett. 2004;93:077402.
[15] Zheng J, Nicovich PR, Dickson RM. Highly fluorescent noble-metal quantum dots. Annu Rev Phys Chem. 2007;58:409–431.
[16] Zheng J, Zhou C, Yu M, et al. Different sized luminescent gold nanoparticles. Nanoscale. 2012;4:4073–4083.
[17] Yu Y, Luo Z, Chevrier DM, et al. Identification of a highly luminescent $Au_{22}(SG)_{18}$ nanocluster. J Am Chem Soc. 2014;136:1246–1249.
[18] Peyser LA, Vinson AE, Bartko AP, et al. Photoactivated fluorescence from individual silver nanoclusters. Science. 2001;291:103–106.
[19] Cremer GD, Coutiño-Gonzalez E, Roeffaers MBJ, et al. Characterization of fluorescence in heat-treated silver-exchanged zeolites. J Am Chem Soc. 2009; 131:3049–3056.
[20] Fenwick O, Coutiño-Gonzalez E, Grandjean D, et al. Tuning the energetics and tailoring the optical properties of silver clusters confined in zeolites. Nat Mater. 2016;15:1017–1022.
[21] Kang X, Zhu M. Tailoring the photoluminescence of atomically precise nanoclusters. Chem Soc Rev. 2019;48:2422–2457.
[22] Chen Y, Yang T, Pan H, et al. Photoemission mechanism of water-soluble silver nanoclusters: ligand-to-metal–metal charge transfer vs strong coupling between surface plasmon and emitters. J Am Chem Soc. 2014;136:1686–1689.
[23] Ziefuss AR, Steenbock T, Benner D, et al. Photoluminescence of fully inorganic colloidal gold

nanocluster and their manipulation using surface charge effects. Adv Mater. 2021;33:2101549.
[24] Wilcoxon JP, Martin JE, Parsapour F, et al. Photoluminescence from nanosize gold clusters. J Chem Phys. 1998;108:9137–9143.
[25] Bigioni TP, Whetten RL, Dag Ö. Near-infrared luminescence from small gold nanocrystals. J Phys Chem B. 2000;104:6983–6986.
[26] Huang T, Murray RW. Visible luminescence of water-soluble monolayer-protected gold clusters. J Phys Chem B. 2001;105:12498–12502.
[27] Li C, Sun P, Ding H, et al. Synthesis of metal nanoclusters and regulation of their photoluminescent properties. Sci Sin Chim. 2021;51:688–702.
[28] Yan J, Teo BK, Zheng N. Surface chemistry of atomically precise coinage-metal nanoclusters: from structural control to surface reactivity and catalysis. Acc Chem Res. 2018;51:3084–3093.
[29] Fang J, Zhang B, Yao Q, et al. Recent advances in the synthesis and catalytic applications of ligand-protected, atomically precise metal nanoclusters. Coord Chem Rev. 2016;322:1–29.
[30] Luo Z, Castleman AW, Khanna SN. Reactivity of metal clusters. Chem Rev. 2016;116:14456–14492.
[31] Wang Y, Wan X-K, Ren L, et al. Atomically precise alkynyl-protected metal nanoclusters as a model catalyst: observation of promoting effect of surface ligands on catalysis by metal nanoparticles. J Am Chem Soc. 2016;138:3278–3281.
[32] Tsunoyama H, Ichikuni N, Sakurai H, et al. Effect of electronic structures of Au clusters stabilized by poly (N-vinyl-2-pyrrolidone) on aerobic oxidation catalysis. J Am Chem Soc. 2009;131:7086–7093.
[33] Wan X-K, Wang J-Q, Nan Z-A, et al. Ligand effects in catalysis by atomically precise gold nanoclusters. Sci Adv. 2017;3:1701823.
[34] Zhang Q-F, Chen X, Wang L-S. Toward solution syntheses of the tetrahedral Au_{20} pyramid and atomically precise gold nanoclusters with uncoordinated sites. Acc Chem Res. 2018;51:2159–2168.
[35] Zhu Y, Qian H, Drake BA, et al. Atomically precise $Au_{25}(SR)_{18}$ nanoparticles as catalysts for the selective hydrogenation of alpha, beta-unsaturated ketones and aldehydes. Angew Chem Int Ed. 2010;49:1295–1298.
[36] Cai X, Hu W, Xu S, et al. Structural relaxation enabled by internal vacancy available in a 24-atom gold cluster reinforces catalytic reactivity. J Am Chem Soc. 2020;142:4141–4153.
[37] Liu L, Corma A. Metal catalysts for heterogeneous catalysis: from single atoms to nanoclusters and nanoparticles. Chem Rev. 2018;118:4981–5079.
[38] Sun Y, Cai X, Hu W, et al. Electrocatalytic and photocatalytic applications of atomically precise gold-based nanoclusters. Sci China Chem. 2020;64:1065–1075.
[39] Kawawaki T, Negishi Y. Gold nanoclusters as electrocatalysts for energy conversion. Nanomaterials. 2020;10:238.
[40] Knoppe S, Bürgi T. Chirality in thiolate-protected gold clusters. Acc Chem Res. 2014;47:1318–1326.
[41] Xia Y, Zhou Y, Tang Z. Chiral inorganic nanoparticles: origin, optical properties and bioapplications. Nanoscale. 2011;3:1374–1382.
[42] Moshe AB, Szwarcman D, Markovich G. Size dependence of chiroptical activity in colloidal quantum dots. ACS Nano. 2011;5:9034–9043.
[43] Li Y, Higaki T, Du X, et al. Chirality and surface bonding correlation in atomically precise metal nanoclusters. Adv Mater. 2020;32:1905488.
[44] Xiao L, An T, Wang L, et al. Novel properties and applications of chiral inorganic nanostructures. Nano Today. 2020;30:100824.
[45] Shen J-S, Li D-H, Zhang M-B, et al. Metal–metal-interaction-facilitated coordination polymer as a sensing ensemble: a case study for cysteine sensing. Langmuir. 2010;27:481–486.
[46] Russier-Antoine I, Bertorelle F, Kulesza A, et al. Chiral supramolecular gold-cysteine nanoparticles: chiroptical and nonlinear optical properties. Prog Nat Sci. 2016;26:455–460.
[47] Si W-D, Li Y-Z, Zhang S-S, et al. Toward controlled syntheses of diphosphine-protected homochiral gold nanoclusters through precursor engineering. ACS Nano. 2021;15:16019–16029.
[48] Pan Y, Han Z, Chen S, et al. Metallic nanoclusters: from synthetic challenges to applications of their unique properties in food contamination detection. Coord Chem Rev. 2023;478:214964.
[49] Bonačić-Koutecký V, Le Guével X, Antoine R. Engineering liganded gold nanoclusters as efficient theranostic agents for cancer applications. Chembiochem. 2022;24:e202200524.
[50] Whetten RL, Khoury JT, Alvarez MM, et al. Nanocrystal gold molecules. Adv Mater. 1996;8:428–433.
[51] Zheng J, Dickson RM. Individual water-soluble dendrimer-encapsulated silver nanodot fluorescence. J Am Chem Soc. 2002;124:13982–13983.
[52] Zhou C, Sun C, Yu M, et al. Luminescent gold nanoparticles with mixed valence states generated from dissociation of polymeric Au(I) thiolates. J Phys Chem C. 2010;114:7727–7732.
[53] Liu J, Duchesne PN, Yu M, et al. Luminescent gold nanoparticles with size-independent emission. Angew Chem Int Ed. 2016;55:8894–8898.
[54] Wu Z, Jin R. On the ligand's role in the fluorescence of gold nanoclusters. Nano Lett. 2010;10:2568–2573.
[55] Luo Z, Yuan X, Yu Y, et al. From aggregation-induced emission of Au(I)-thiolate complexes to ultrabright Au(0)@Au(I)-thiolate core-shell nanoclusters. J Am Chem Soc. 2012;134:16662–16670.
[56] Wu Z, Yao Q, Jin O, et al. Unraveling the impact of gold(I)–thiolate motifs on the aggregation induced emission of gold nanoclusters. Angew Chem Int Ed. 2020;132:10020–10025.
[57] Zeng Y, Havenridge S, Gharib M, et al. Impact of ligands on structural and optical properties of Ag29 nanoclusters. J Am Chem Soc. 2021;143:9405–9414.
[58] Sahoo K, Chakraborty I. Ligand effects on photoluminescence of atomically precise silver nanoclusters. Nanoscale. 2023. DOI:10.1039/D1032NR06619J
[59] Barik SK, Chen C-Y, Chiu T-H, et al. Surface modifications of eight-electron palladium silver superatomic alloys. Commun Chem. 2022;5:1–12.
[60] Ding M, Tang L, Ma X, et al. Effects of ligand tuning and core doping of atomically precise copper nanoclusters on CO_2 electroreduction selectivity. Commun Chem. 2022;5:1–8.
[61] Kolay S, Bain D, Maity S, et al. Self-assembled metal nanoclusters: driving forces and structural correlation with optical properties. Nanomaterials. 2022;12:544.

[62] Parker JF, Fields-Zinna AC, Murray RW. The story of a monodisperse gold nanoparticle: $Au_{25}L_{18}$. Acc Chem Res. 2010;43:1289–1296.
[63] Yang T-Q, Peng B, Shan B-Q, et al. Origin of the photoluminescence of metal nanoclusters: from metal-centered emission to ligand-centered emission. Nanomaterials. 2020;10:261.
[64] Roduner E. Size matters: why nanomaterials are different. Chem Soc Rev. 2006;35:583–592.
[65] Hartland GV. Optical studies of dynamics in noble metal nanostructures. Chem Rev. 2011;111:3858–3887.
[66] Jin R. Quantum sized, thiolate-protected gold nanoclusters. Nanoscale. 2010;2:343–362.
[67] Diez I, Ras RH. Fluorescent silver nanoclusters. Nanoscale. 2011;3:1963–1970.
[68] Lu Y, Chen W. Sub-nanometre sized metal clusters: from synthetic challenges to the unique property discoveries. Chem Soc Rev. 2012;41:3594–3623.
[69] Yau SH, Varnavski O, III TG. An ultrafast look at Au nanoclusters. Acc Chem Res. 2013;46:1506–1516.
[70] Goswami N, Yao Q, Chen T, et al. Mechanistic exploration and controlled synthesis of precise thiolate-gold nanoclusters. Coord Chem Rev. 2016;329:1–15.
[71] Zhou M, Du X, Wang H, et al. The critical number of gold atoms for a metallic state nanocluster: resolving a decades-long question. ACS Nano. 2021;15:13980–13992.
[72] Jin R, Higaki T. Open questions on the transition between nanoscale and bulk properties of metals. Commun Chem. 2021;4:1–4.
[73] Whetten RL, Price RC. Nano-golden order. Science. 2007;318:430–433.
[74] Quintanilla M, Liz-Marzan LM. Caged clusters shine brighter. Science. 2018;361:645.
[75] Zhou M, Song Y. Origins of visible and near-infrared emissions in $[Au_{25}(SR)_{18}]^-$ nanoclusters. J Phys Chem Lett. 2021;12:1514–1519.
[76] Mooradian A. Photoluminescence of metals. Phys Rev Lett. 1969;22:185–187.
[77] Link S, Beeby A, FitzGerald S, et al. Visible to infrared luminescence from a 28-atom gold cluster. J Phys Chem B. 2002;106:3410–3415.
[78] Boyd GT, Yu ZH, Shen YR. Photoinduced luminescence from the noble metals and its enhancement on roughened surfaces. Phys Rev B Condens Matter. 1986;33:7923–7936.
[79] Mohamed MB, Volkov V, Link S, et al. The 'lightning' gold nanorods: fluorescence enhancement of over a million compared to the gold metal. Chem Phys Lett. 2000;317:517–523.
[80] Alvarez MM, Khoury JT, Schaaff TG, et al. Optical absorption spectra of nanocrystal gold molecules. J Phys Chem B. 1997;101:3706–3712.
[81] Shichibu Y, Negishi Y, Tsunoyama H, et al. Extremely high stability of glutathionate-protected Au25 clusters against core etching. Small. 2007;3:835–839.
[82] Cha S-H, Kim J-U, Kim K-H, et al. Preparation and photoluminescent properties of gold(I)-alkanethiolate complexes having highly ordered supramolecular structures. Chem Mater. 2007;19:6297–6303.
[83] Richards CI, Choi S, Hsiang J-C, et al. Oligonucleotide-stabilized Ag nanocluster fluorophores. J Am Chem Soc. 2008;130:5038–5039.
[84] Xie J, Zheng Y, Ying JY. Protein-directed synthesis of highly fluorescent gold nanoclusters. J Am Chem Soc. 2009;131:888–889.
[85] Antoine R, Maysinger D, Sancey L, et al. Open questions on proteins interacting with nanoclusters. Commun Chem. 2022;5:1–5.
[86] Ungor, Dékány, Csapó. Reduction of tetrachloroaurate(III) ions with bioligands: role of the thiol and amine functional groups on the structure and optical features of gold nanohybrid systems. Nanomaterials. 2019;9:1229.
[87] Kawawaki T, Mori Y, Wakamatsu K, et al. Controlled colloidal metal nanoparticles and nanoclusters: recent applications as cocatalysts for improving photocatalytic water-splitting activity. J Mater Chem A. 2020;8:16081–16113.
[88] Luo J, Xie Z, Lam JWY, et al. Aggregation-induced emission of 1-methyl-1,2,3,4,5-pentaphenylsilole. Chem Commun. 2001;18:1740–1741.
[89] Veselska O, Okhrimenko L, Guillou N, et al. An intrinsic dual-emitting gold thiolate coordination polymer, $[Au(+I)(p\text{-}SPhCO_2H)]_n$, for ratiometric temperature sensing. J Mater Chem C. 2017;5:9843–9848.
[90] Lavenn C, Okhrimenko L, Guillou N, et al. A luminescent double helical gold(i)–thiophenolate coordination polymer obtained by hydrothermal synthesis or by thermal solid-state amorphous-to-crystalline isomerization. J Mater Chem C. 2015;3:4115–4125.
[91] Lavenn C, Guillou N, Monge M, et al. Shedding light on an ultra-bright photoluminescent lamellar gold thiolate coordination polymer $[Au(p\text{-}SPhCO_2Me)]_n$. Chem Commun. 2016;52:9063–9066.
[92] Veselska O, Demessence A. D10 coinage metal organic chalcogenolates: from oligomers to coordination polymers. Coord Chem Rev. 2018;355:240–270.
[93] Su X, Liu J. Ph-guided self-assembly of copper nanoclusters with aggregation-induced emission. ACS Appl Mater Interfaces. 2017;9:3902–3910.
[94] Goswami N, Yao Q, Luo Z, et al. Luminescent metal nanoclusters with aggregation-induced emission. J Phys Chem Lett. 2016;7:962–975.
[95] Jia X, Li J, Wang E. Cu nanoclusters with aggregation induced emission enhancement. Small. 2013;9:3873–3879.
[96] Kang X, Wang S, Zhu M. Observation of a new type of aggregation-induced emission in nanoclusters. Chem Sci. 2018;9:3062–3068.
[97] Chang H, Karan NS, Shin K, et al. Highly fluorescent gold cluster assembly. J Am Chem Soc. 2021;143:326–334.
[98] George A, Maman MP, Bhattacharyya K, et al. Aggregation induced non-emissive-to-emissive switching of molecular platinum clusters. Nanoscale. 2019;11:5914–5919.
[99] Wu Z, Liu J, Gao Y, et al. Assembly-induced enhancement of Cu nanoclusters luminescence with mechanochromic property. J Am Chem Soc. 2015;137:12906–12913.
[100] Mei J, Hong Y, Lam JW, et al. Aggregation-induced emission: the whole is more brilliant than the parts. Adv Mater. 2014;26:5429–5479.
[101] Mei J, Leung NL, Kwok RT, et al. aggregation-induced emission: together we shine, united we soar! Chem Rev. 2015;115:11718–11940.
[102] Zhang H, Zhao Z, McGonigal PR, et al. Clusterization-triggered emission: uncommon luminescence from common materials. Mater Today. 2020;32:275–292.

[103] Zhou J, Yang T, Peng B, et al. Structural water molecules confined in soft and hard nanocavities as bright color emitters. ACS Phys Chem Au. 2022;2:47–58.
[104] Schmidbaur H, Schier A. A briefing on aurophilicity. Chem Soc Rev. 2008;37:1931–1951.
[105] Wang N, Sun Q, Yu J. Ultrasmall metal nanoparticles confined within crystalline nanoporous materials: a fascinating class of nanocatalysts. Adv Mater. 2018;31:1803966.
[106] Chai Y, Shang W, Li W, et al. Noble metal particles confined in zeolites: synthesis, characterization, and applications. Adv Sci. 2019;6:1900299.
[107] Simo A, Polte J, Pfander N, et al. Formation mechanism of silver nanoparticles stabilized in glassy matrices. J Am Chem Soc. 2012;134:18824–18833.
[108] Kuznetsov AS, Tikhomirov VK, Shestakov MV, et al. Ag nanocluster functionalized glasses for efficient photonic conversion in light sources, solar cells and flexible screen monitors. Nanoscale. 2013;5:10065–10075.
[109] De Cremer G, Antoku Y, Roeffaers MB, et al. Photoactivation of silver-exchanged zeolite a. Angew Chem Int Ed. 2008;47:2813–2816.
[110] Coutino-Gonzalez E, Grandjean D, Roeffaers M, et al. X-ray irradiation-induced formation of luminescent silver clusters in nanoporous matrices. Chem Commun. 2014;50:1350–1352.
[111] Altantzis T, Coutino-Gonzalez E, Baekelant W, et al. Direct observation of luminescent silver clusters confined in faujasite zeolites. ACS Nano. 2016;10:7604–7611.
[112] Lin H, Imakita K, Fujii M. Reversible emission evolution from Ag activated zeolite Na-A upon dehydration/hydration. Appl Phys Lett. 2014;105:211903.
[113] Baekelant W, Aghakhani S, Coutino-Gonzalez E, et al. Shaping the optical properties of silver clusters inside zeolite a via guest-host-guest interactions. J Phys Chem Lett. 2018;9:5344–5350.
[114] Coutiño-Gonzalez E, Baekelant W, Grandjean D, et al. Thermally activated LTA(Li)–Ag zeolites with water-responsive photoluminescence properties. J Mater Chem C. 2015;3:11857–11867.
[115] Aghakhani S, Grandjean D, Baekelant W, et al. Atomic scale reversible opto-structural switching of few atom luminescent silver clusters confined in LTA zeolites. Nanoscale. 2018;10:11467–11476.
[116] Lin H, Imakita K, Fujii M, et al. Visible emission from Ag(+) exchanged SOD zeolites. Nanoscale. 2015;7:15665–15671.
[117] Perić M, Sanader Maršić Ž, Russier-Antoine I, et al. Ligand shell size effects on one- and two-photon excitation fluorescence of zwitterion functionalized gold nanoclusters. Phys Chem Chem Phys. 2019;21:23916–23921.
[118] Yang T, Dai S, Yang S, et al. Interfacial clustering-triggered fluorescence–phosphorescence dual solvoluminescence of metal nanoclusters. J Phys Chem Lett. 2017;8:3980–3985.
[119] Yang T, Dai S, Tan H, et al. Mechanism of photoluminescence in Ag nanoclusters: metal-centered emission versus synergistic effect in ligand-centered emission. J Phys Chem C. 2019;123:18638–18645.
[120] Yang T, Shan B, Huang F, et al. P band intermediate state (PBIS) tailors photoluminescence emission at confined nanoscale interface. Commun Chem. 2019;2:1–11.
[121] Peng B, Zhang K. Origin of the bright photoluminescence of thiolate-protected gold nanoclusters: confined structural water molecules as real emitters. ChemRxiv. 2021. DOI:10.26434/chemrxiv-22021-zp26439z26433
[122] Peng B, Zheng L-X, Wang P-Y, et al. Physical origin of dual-emission of Au–Ag bimetallic nanoclusters. Front Chem. 2021;9:756993.
[123] Yang T-Q, Hu X-D, Shan B-Q, et al. Caged structural water molecules emit tunable brighter colors by topological excitation. Nanoscale. 2021;13:15058–15066.
[124] Yang T, Zhou J, Shan B, et al. Hydrated hydroxide complex dominates the AIE properties of nonconjugated polymeric luminophores. Macromol Rapid Commun. 2022;43:2100720.
[125] Ewles J. Water as an activator of luminescence. Nature. 1930;125:706–707.
[126] Przibram K. Fluorescence of adsorbed water. Nature. 1958;182:520–520.
[127] Tan H, Zhou H, Zhao Y, et al. Regulation of silver nanoclusters with 4 orders of magnitude variation of fluorescence lifetimes with solvent-induced noncovalent interaction. J Phys Chem C. 2022;126:5198–5205.
[128] Hu X-D, Shan B-Q, Tao R, et al. Interfacial hydroxyl promotes the reduction of 4-nitrophenol by ag-based catalysts confined in dendritic mesoporous silica nanospheres. J Phys Chem C. 2021;125:2446–2453.
[129] Shan BQ, Zhou JF, Ding M, et al. Surface electronic states mediate concerted electron and proton transfer at metal nanoscale interfaces for catalytic hydride reduction of -NO_2 to -NH_2. Phys Chem Chem Phys. 2021;23:12950–12957.
[130] Tao R, Shan B-Q, Sun H-D, et al. Surface molecule manipulated Pt/TiO_2 catalysts for selective hydrogenation of cinnamaldehyde. J Phys Chem C. 2021;125:13304–13312.
[131] Ding M, Shan B-Q, Peng B, et al. Dynamic Pt–OH^-·H_2O–Ag species mediate coupled electron and proton transfer for catalytic hydride reduction of 4-nitrophenol at the confined nanoscale interface. Phys Chem Chem Phys. 2022;24:7923–7936.
[132] Wang P-Y, Zhou J-F, Chen H, et al. Activation of H_2O tailored by interfacial electronic states at a nanoscale interface for enhanced electrocatalytic hydrogen evolution. JACS Au. 2022;2:1457–1471.
[133] Zheng L-X, Peng B, Zhou J-F, et al. High efficient and stable thiol-modified dendritic mesoporous silica nanospheres supported gold catalysts for gas-phase selective oxidation of benzyl alcohol with ultra-long lifetime. Microporous Mesoporous Mater. 2022;342:112140.
[134] Lebastard C, Wilmet M, Cordier S, et al. High performance {Nb_5TaX_{12}}@PVP (X = Cl, Br) cluster-based nanocomposites coatings for solar glazing applications. Sci Technol Adv Mater. 2022;23:446–456.
[135] Nguyen NTK, Lebastard C, Wilmet M, et al. A review on functional nanoarchitectonics nanocomposites based on octahedral metal atom clusters (Nb_6, Mo_6, Ta_6, W_6, Re_6): inorganic 0D and 2D powders and films. Sci Technol Adv Mater. 2022;23:547–578.
[136] Gholipour-Ranjbar H, Deepika, Jena P, et al. Gas-phase fragmentation of single heteroatom-incorporated $Co_5MS_8(PEt_3)^{6+}$ (M = mn, Fe, Co, Ni) nanoclusters. Commun Chem. 2022;5:1–8.

[137] He M, Zhang K, Guan Y, et al. Green carbon science: fundamental aspects. Natl Sci Rev. 2023;nwad046. DOI:10.1093/nsr/nwad1046
[138] Hu Z, Shu Y, Qin H, et al. Water effects on colloidal semiconductor nanocrystals: correlation of photophysics and photochemistry. J Am Chem Soc. 2021;143:18721–18732.
[139] Li J, Cao W, Shu Y, et al. Water molecules bonded to the carboxylate groups at the inorganic–organic interface of an inorganic nanocrystal coated with alkanoate ligands. Natl Sci Rev. 2022;9:1–10.
[140] Baker SN, Baker GA. Luminescent carbon nanodots: emergent nanolights. Angew Chem Int Ed. 2010;49:6726–6744.
[141] Lim SY, Shen W, Gao Z. Carbon quantum dots and their applications. Chem Soc Rev. 2015;44:362–381.
[142] Zheng XT, Ananthanarayanan A, Luo KQ, et al. Glowing graphene quantum dots and carbon dots: properties, syntheses, and biological applications. Small. 2015;11:1620–1636.
[143] Wang Y, Hu A. Carbon quantum dots: synthesis, properties and applications. J Mater Chem C. 2014;2:6921–6939.
[144] Zhu S, Song Y, Zhao X, et al. The photoluminescence mechanism in carbon dots (graphene quantum dots, carbon nanodots, and polymer dots): current state and future perspective. Nano Res. 2015;8:355–381.
[145] Fu Y, Zhu H, Chen J, et al. Metal halide perovskite nanostructures for optoelectronic applications and the study of physical properties. Nat Rev Mater. 2019;4:169–188.
[146] Akkerman QA, Rainò G, Kovalenko MV, et al. Genesis, challenges and opportunities for colloidal lead halide perovskite nanocrystals. Nat Mater. 2018;17:394–405.
[147] Chouhan L, Ghimire S, Subrahmanyam C, et al. Synthesis, optoelectronic properties and applications of halide perovskites. Chem Soc Rev. 2020;49:2869–2885.
[148] Alivisatos A. Semiconductor clusters, nanocrystals, and quantum dots. Science. 1996;271:933–937.
[149] Zhang Q, Yin Y. All-inorganic metal halide perovskite nanocrystals: opportunities and challenges. ACS Cent Sci. 2018;4:668–679.
[150] Manser JS, Christians JA, Kamat PV. Intriguing optoelectronic properties of metal halide perovskites. Chem Rev. 2016;116:12956–13008.
[151] Liu L, Pan K, Xu K, et al. Impact of molecular ligands in the synthesis and transformation between metal halide perovskite quantum dots and magic sized clusters. ACS Phys Chem Au. 2022;2:156–170.
[152] Win AA, Chou K-C, Zeitz DC, et al. Origin of the near 400 nm absorption and emission band in the synthesis of cesium lead bromide nanostructures: metal halide molecular clusters rather than perovskite magic-sized clusters. J Phys Chem Lett. 2022;14:116–121.
[153] Tsien RY. The green fluorescent protein. Annu Rev Biochem. 1998;67:509–544.
[154] Baird GS, Zacharias DA, Tsien RY. Circular permutation and receptor insertion within green fluorescent proteins. Proc Natl Acad Sci USA. 1999;96:11241–11246.
[155] Yoshida K, Uwada K, Kumaoka H, et al. Fluorescence sensing behavior of crystals of an imidazole-type clathrate host upon contact with gaseous carboxylic acids. Chem Lett. 2001;30:808–809.
[156] Zhang J, Campbell RE, Ting AY, et al. Creating new fluorescent probes for cell biology. Nat Rev Mol Cell Biol. 2002;3:906–918.
[157] Craggs TD. Green fluorescent protein: structure, folding and chromophore maturation. Chem Soc Rev. 2009;38:2865.
[158] Dong J, Solntsev KM, Tolbert LM. Activation and tuning of green fluorescent protein chromophore emission by alkyl substituent-mediated crystal packing. J Am Chem Soc. 2009;131:662–670.
[159] Sample V, Newman RH, Zhang J. The structure and function of fluorescent proteins. Chem Soc Rev. 2009;38:2852.
[160] Zimmer M. GFP: from jellyfish to the Nobel prize and beyond. Chem Soc Rev. 2009;38:2823–2832.
[161] Tou S-L, Huang G-J, Chen P-C, et al. Aggregation-induced emission of GFP-like chromophores via exclusion of solvent–solute hydrogen bonding. Chem Commun. 2014;50:620–622.
[162] Laptenok SP, Gil AA, Hall CR, et al. Infrared spectroscopy reveals multi-step multi-timescale photoactivation in the photoconvertible protein archetype dronpa. Nat Chem. 2018;10:845–852.
[163] Woodhouse J, Nass Kovacs G, Coquelle N, et al. Photoswitching mechanism of a fluorescent protein revealed by time-resolved crystallography and transient absorption spectroscopy. Nat Commun. 2020;11:741.